

- 16.1 *The Discovery of Sirius B*
- 16.2 *White Dwarfs*
- 16.3 *The Physics of Degenerate Matter*
- 16.4 *The Chandrasekhar Limit*
- 16.5 *The Cooling of White Dwarfs*
- 16.6 *Neutron Stars*
- 16.7 *Pulsars*

### 16.1 ■ THE DISCOVERY OF SIRIUS B

In 1838 Friedrich Wilhelm Bessel (1784–1846) used the technique of stellar parallax to find the distance to the star 61 Cygni. Following this first successful measurement of a stellar distance, Bessel applied his talents to another likely candidate: Sirius, the brightest appearing star in the sky. Its parallax angle of  $p'' = 0.379''$  corresponds to a distance of only 2.64 pc, or 8.61 ly (see Appendix E). Sirius's brilliance in the night sky is due in part to its proximity to Earth. As he followed the star's path through the heavens, Bessel found that it deviated slightly from a straight line. After ten years of precise observations, Bessel concluded in 1844 that Sirius is actually a binary star system. Although unable to detect the companion of the brighter star, he deduced that its orbital period was about 50 years (the modern value is 49.9 years) and predicted its position. The search was on for the unseen "Pup," the faint companion of the luminous "Dog Star."

The telescopes of Bessel's time were incapable of finding the Pup so close to the glare of its bright counterpart, and following Bessel's death in 1846 the enthusiasm for the quest waned. Finally, in 1862, Alvan Graham Clark (1832–1897), son of the prominent American lensmaker Alvan Clark (1804–1887), tested his father's new 18-inch refractor (3 inches larger than any previous instrument) on Sirius, and he promptly discovered the Pup at its predicted position. The dominant Sirius A was found to be nearly one thousand times brighter than the Pup, now called Sirius B; see Fig. 16.1. The details of their orbits about their center of mass (see Fig. 16.2 and Problem 7.4) revealed that Sirius A and Sirius B have masses of about  $2.3 M_{\odot}$  and  $1.0 M_{\odot}$ , respectively. A more recent determination for the mass of Sirius B is  $1.053 \pm 0.028 M_{\odot}$ , and it is this value that we will use.

Clark's discovery of Sirius B was made near the opportune time of apastron, when the two stars were most widely separated (by just  $10''$ ). The great difference in their luminosities ( $L_A = 23.5 L_{\odot}$  and  $L_B = 0.03 L_{\odot}$ ) makes observations at other times much more difficult.

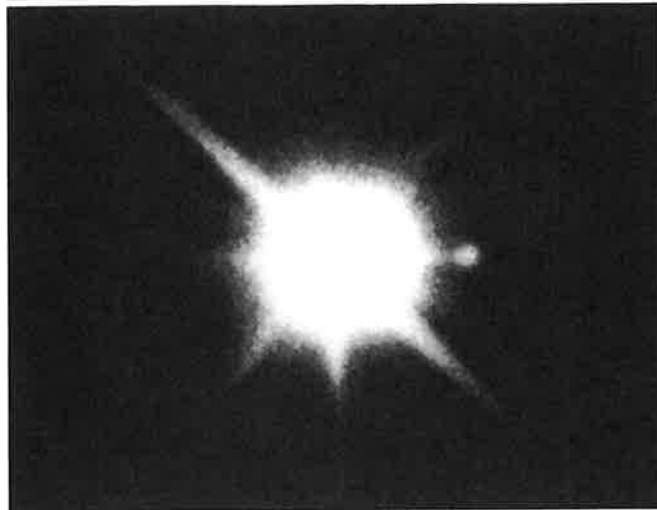


**FIGURE 16.1** The white dwarf, Sirius B, beside the overexposed image of Sirius A. (Courtesy of Lick Observatory.)

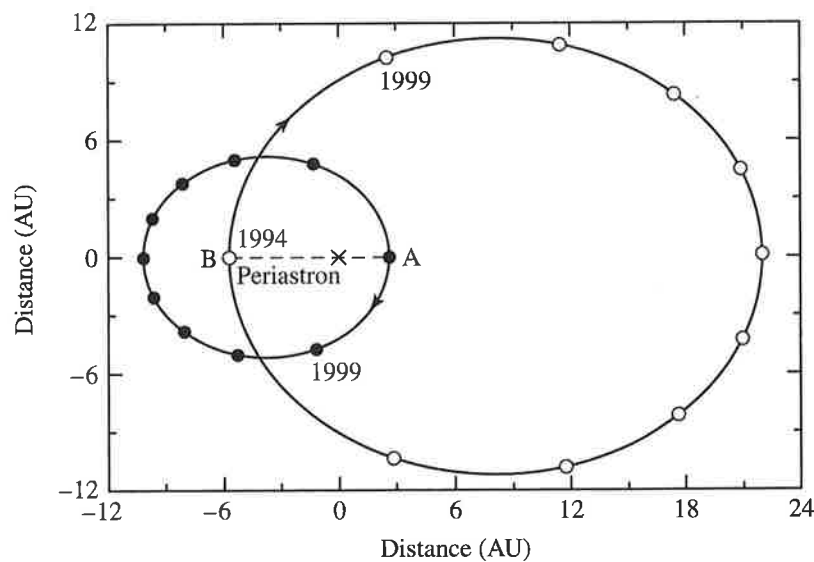


**FIGURE 16.2** The orbits of Sirius A and Sirius B. The center of mass of the system is marked with an “x.”

When the next apastron arrived 50 years later, spectroscopists had developed the tools to measure the stars’ surface temperatures. From the Pup’s faint appearance, astronomers expected it to be cool and red. They were startled when Walter Adams (1876–1956), working at Mt. Wilson Observatory in 1915, discovered that, to the contrary, Sirius B is a hot, blue-white star that emits much of its energy in the ultraviolet. A modern value of the temperature of Sirius B is 27,000 K, much hotter than Sirius A’s 9910 K.

The implications for the star’s physical characteristics were astounding. Using the Stefan–Boltzmann law, Eq. (3.17), to calculate the size of Sirius B results in a radius of only  $5.5 \times 10^6 \text{ m} \approx 0.008 R_{\odot}$ . Sirius B has the mass of the Sun confined within a volume smaller than Earth! The average density of Sirius B is  $3.0 \times 10^9 \text{ kg m}^{-3}$ , and the acceler-

ation due to gravity at its surface is about  $4.6 \times 10^6 \text{ m s}^{-2}$ . On Earth, the pull of gravity on a teaspoon of white-dwarf material would be  $1.45 \times 10^5 \text{ N}$  (over 16 tons), and on the surface of the white dwarf it would weigh 470,000 times more. This fierce gravity reveals itself in the spectrum of Sirius B; it produces an immense pressure near the surface that results in very broad hydrogen absorption lines; see Fig. 8.15.<sup>1</sup> Apart from these lines, its spectrum is a featureless continuum.

Astronomers first reacted to the discovery of Sirius B by dismissing the results, calling them “absurd.” However, the calculations are so simple and straightforward that this attitude soon changed to the one expressed by Eddington in 1922: “Strange objects, which persist in showing a type of spectrum entirely out of keeping with their luminosity, may ultimately teach us more than a host which radiate according to rule.” Like all sciences, astronomy advances most rapidly when confronted with exceptions to its theories.

## 16.2 ■ WHITE DWARFS

Obviously Sirius B is not a normal star. It is a **white dwarf**, a class of stars that have approximately the mass of the Sun and the size of Earth. Although as many as one-quarter of the stars in the vicinity of the Sun may be white dwarfs, the average characteristics of these faint stars have been difficult to determine because a complete sample has been obtained only within 10 pc of the Sun.

### Classes of White Dwarf Stars

Figures 8.14 and 8.16 show that the white dwarfs occupy a narrow sliver of the H–R diagram that is roughly parallel to and below the main sequence. Although white dwarfs are typically whiter than normal stars, the name itself is something of a misnomer since they come in all colors, with surface temperatures ranging from less than 5000 K to more than 80,000 K. Their spectral type, D (for “dwarf”), has several subdivisions. The largest group (about two-thirds of the total number, including Sirius B), called **DA white dwarfs**, display only pressure-broadened hydrogen absorption lines in their spectra. Hydrogen lines are absent from the **DB white dwarfs** (8%), which show only helium absorption lines, and the **DC white dwarfs** (14%) show no lines at all—only a continuum devoid of features. The remaining types include **DQ white dwarfs**, which exhibit carbon features in their spectra, and **DZ white dwarfs** with evidence of metal lines.

### Central Conditions in White Dwarfs

It is instructive to estimate the conditions at the center of a white dwarf of mass  $M_{\text{wd}}$  and radius  $R_{\text{wd}}$ , using the values for Sirius B given in the preceding section. Equation (14.5) with  $r = 0$  shows that the central pressure is roughly<sup>2</sup>

$$P_c \approx \frac{2}{3} \pi G \rho^2 R_{\text{wd}}^2 \approx 3.8 \times 10^{22} \text{ N m}^{-2}, \quad (16.1)$$

<sup>1</sup>Recall the discussion of pressure broadening in Section 9.5.

<sup>2</sup>Remember that Eq. (14.5) was obtained for the unrealistic assumption of constant density.

about 1.5 million times larger than the pressure at the center of the Sun. A crude estimate of the central temperature may be obtained from Eq. (10.68) for the radiative temperature gradient,<sup>3</sup>

$$\frac{dT}{dr} = -\frac{3}{4ac} \frac{\bar{\kappa}\rho}{T^3} \frac{L_r}{4\pi r^2}$$

or

$$\frac{T_{\text{wd}} - T_c}{R_{\text{wd}} - 0} = -\frac{3}{4ac} \frac{\bar{\kappa}\rho}{T_c^3} \frac{L_{\text{wd}}}{4\pi R_{\text{wd}}^2}.$$

Assuming that the surface temperature,  $T_{\text{wd}}$ , is much smaller than the central temperature and using  $\bar{\kappa} = 0.02 \text{ m}^2 \text{ kg}^{-1}$  for electron scattering (Eq. 9.27 with  $X = 0$ ) give

$$T_c \approx \left[ \frac{3\bar{\kappa}\rho}{4ac} \frac{L_{\text{wd}}}{4\pi R_{\text{wd}}^2} \right]^{1/4} \approx 7.6 \times 10^7 \text{ K}.$$

Thus the central temperature of a white dwarf is several times  $10^7$  K.

These estimated values for a white dwarf lead directly to a surprising conclusion. Although hydrogen makes up roughly 70% of the visible mass of the universe, it cannot be present in appreciable amounts below the surface layers of a white dwarf. Otherwise, the dependence of the nuclear energy generation rates on density and temperature (see Eq. 10.46 for the pp chain and Eq. 10.58 for the CNO cycle) would produce white dwarf luminosities several orders of magnitude larger than those actually observed. Similar reasoning applied to other reaction sequences implies that thermonuclear reactions are not involved in producing the energy radiated by white dwarfs and that their centers must therefore consist of particles that are incapable of fusion at these densities and temperatures.

As was discussed in Section 13.2, white dwarfs are manufactured in the cores of low- and intermediate-mass stars (those with an initial mass below 8 or 9  $M_{\odot}$  on the main sequence) near the end of their lives on the asymptotic giant branch of the H-R diagram. Because any star with a helium core mass exceeding about 0.5  $M_{\odot}$  will undergo fusion, most white dwarfs consist primarily of completely ionized carbon and oxygen nuclei.<sup>4</sup> As the aging giant expels its surface layers as a planetary nebula, the core is exposed as a white dwarf progenitor. The distribution of DA white dwarf masses is sharply peaked at 0.56  $M_{\odot}$ , with some 80% lying between 0.42  $M_{\odot}$  and 0.70  $M_{\odot}$ ; see Fig. 16.3. The much larger main-sequence masses quoted earlier imply that significant amounts of mass loss occurred while on the asymptotic giant branch, involving thermal pulses and a superwind.

### Spectra and Surface Composition

The exceptionally strong pull of the white dwarf's gravity is responsible for the characteristic hydrogen spectrum of DA white dwarfs. Heavier nuclei are pulled below the surface while

<sup>3</sup>As we will discuss later in Section 16.5, the assumption of a radiative temperature gradient is incorrect because the energy is actually carried outward by electron conduction. However, Eq. (10.68) is sufficient for the purpose of this estimation.

<sup>4</sup>Low-mass helium white dwarfs may also exist, and rare oxygen-neon-magnesium white dwarfs have been detected in a few novae.

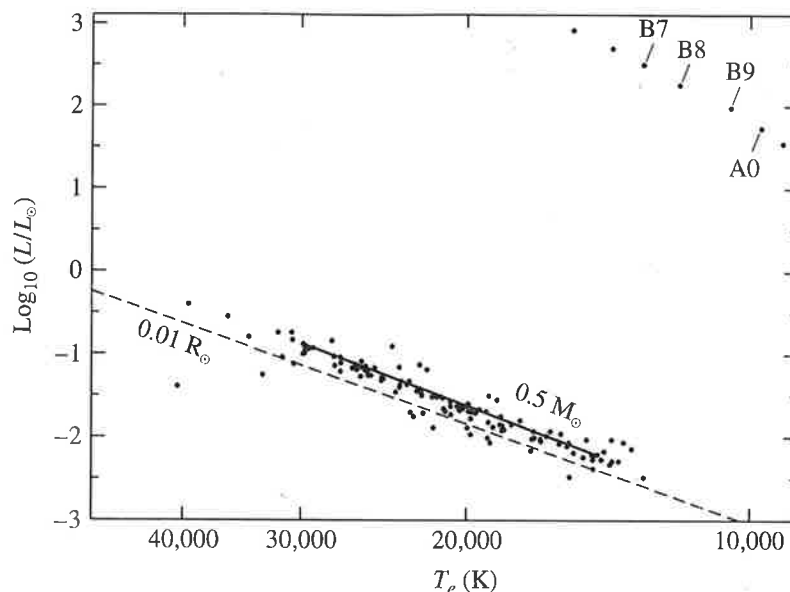


**FIGURE 16.3** DA white dwarfs on an H–R diagram. A line marks the location of the  $0.50 M_{\odot}$  white dwarfs, and a portion of the main sequence is at the upper right. (Data from Bergeron, Saffer, and Liebert, *Ap. J.*, 394, 228, 1992.)

the lighter hydrogen rises to the top, resulting in a thin outer layer of hydrogen covering a layer of helium on top of the carbon–oxygen core.<sup>5</sup> This vertical stratification of nuclei according to their mass takes only 100 years or so in the hot atmosphere of the star. The origin of the non-DA (e.g., DB and DC) white dwarfs is not yet clear. Efficient mass-loss may occur on the asymptotic giant branch associated with the thermal pulse or superwind phases, stripping the white dwarf of nearly all of its hydrogen. Alternatively, a single white dwarf may be transformed between the DA and non-DA spectral types by convective mixing in its surface layers.<sup>6</sup> For example, the helium convection zone’s penetration into a thin hydrogen layer above could change a DA into a DB white dwarf by diluting the hydrogen with additional helium.

### Pulsating White Dwarfs

White dwarfs with surface temperatures of  $T_e \approx 12,000$  K lie within the instability strip of the H–R diagram and pulsate with periods between 100 and 1000 s; see Fig. 8.16 and Table 14.1. These **ZZ Ceti** variables, named after the prototype discovered in 1968 by Arlo Landolt, are variable DA white dwarfs; hence they are also known as **DAV stars**. The pulsation periods correspond to nonradial g-modes that resonate within the white dwarf’s surface layers of hydrogen and helium.<sup>7</sup> Because these g-modes involve almost perfectly

<sup>5</sup>Estimates of the relative masses of the hydrogen and helium layers range from  $m(\text{H})/m(\text{He}) \approx 10^{-2}$  to  $10^{-11}$  for DA white dwarfs.

<sup>6</sup>As we will see in Section 16.5, steep temperature gradients produce convection zones in the white dwarf’s surface layers.

<sup>7</sup>The nonradial pulsation of stars was discussed in Section 14.4. Unlike the g-modes of normal stars, shown in Fig. 14.18, the g-modes of white dwarfs are confined to their surface layers.

horizontal displacements, the radii of these compact pulsators hardly change. Their brightness variations (typically a few tenths of a magnitude) are due to temperature variations on the stars' surfaces. Since most stars will end their lives as white dwarfs, these must be the most common type of variable star in the universe, although only about seventy had been detected at the time this text was written.

Successful numerical calculations of pulsating white dwarf models were carried out by American astronomer Don Winget and others. They were able to demonstrate that it is the *hydrogen* partial ionization zone that is responsible for driving the oscillations of the ZZ Ceti stars, as mentioned in Section 14.2. These computations also confirmed the elemental stratification of white dwarf envelopes. Winget and his colleagues went on to predict that hotter DB white dwarfs should also exhibit g-mode oscillations driven by the *helium* partial ionization zone. Within a year's time, this prediction was confirmed when the first **DBV** star ( $T_e \approx 27,000$  K) was discovered by Winget and his collaborators.<sup>8</sup> The location of the DAV and DBV stars on the H–R diagram is shown in Fig. 16.4, along with the very hot DOV and PNNV ( $T_e \approx 10^5$  K) variables that are associated with the birth of white dwarfs. (“PNN” stands for planetary nebula nuclei and the DO spectral type marks the

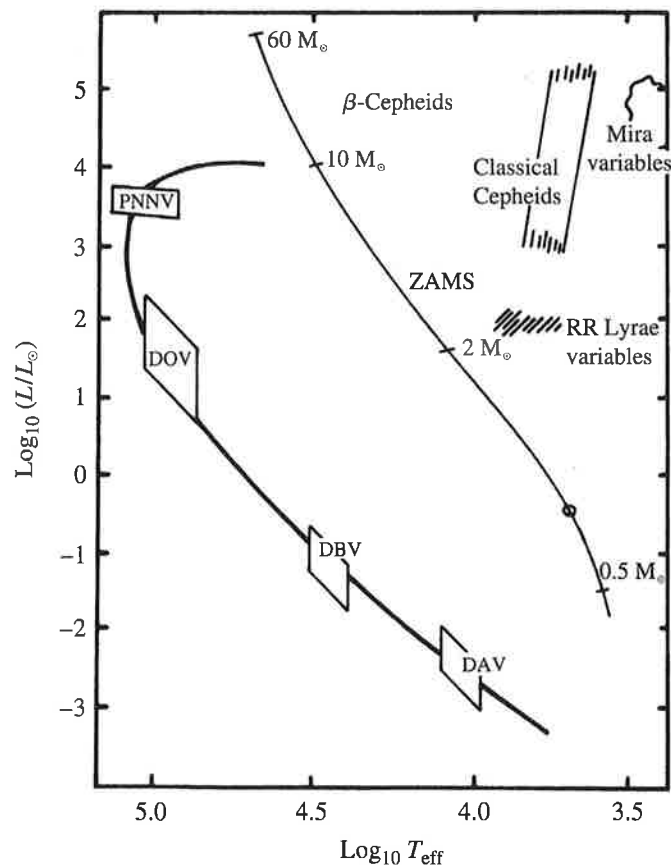


**FIGURE 16.4** Compact pulsators on the H–R diagram. (Figure adapted from Winget, *Advances in Helio- and Asteroseismology*, Christensen-Dalsgaard and Frandsen (eds.), Reidel, Dordrecht, 1988.)

<sup>8</sup>Readers interested in this unique prediction and in the subsequent discovery of a new type of star are referred to Winget et al. (1982a,b).

transition to the white dwarf stage.) All of these stars have multiple periods, simultaneously displaying at least 3, and as many as 125, different frequencies. Astronomers are deciphering the data to obtain a detailed look at the structure of white dwarfs.

### 16.3 ■ THE PHYSICS OF DEGENERATE MATTER

We now delve below the surface to ask, What can support a white dwarf against the relentless pull of its gravity? It is easy to show (Problem 16.4) that normal gas and radiation pressure are completely inadequate. The answer was discovered in 1926 by the British physicist Sir Ralph Howard Fowler (1889–1944), who applied the new idea of the Pauli exclusion principle (recall Section 5.4) to the electrons within the white dwarf. The qualitative argument that follows elucidates the fundamental physics of the **electron degeneracy pressure** described by Fowler.

#### The Pauli Exclusion Principle and Electron Degeneracy

Any system—whether an atom of hydrogen, an oven filled with blackbody photons, or a box filled with gas particles—consists of quantum states that are identified by a set of quantum numbers. Just as the oven is filled with standing waves of electromagnetic radiation that are described by three quantum numbers (specifying the number of photons of wavelength  $\lambda$  traveling in the  $x$ -,  $y$ -, and  $z$ -directions), a box of gas particles is filled with standing de Broglie waves that are also described by three quantum numbers (specifying the particle's component of momentum in each of three directions). If the gas particles are fermions (such as electrons or neutrons), then the Pauli exclusion principle allows at most one fermion in each quantum state because no two fermions can have the same set of quantum numbers.

In an everyday gas at standard temperature and pressure, only one of every  $10^7$  quantum states is occupied by a gas particle, and the limitations imposed by the Pauli exclusion principle become insignificant. Ordinary gas has a *thermal* pressure that is related to its temperature by the ideal gas law. However, as energy is removed from the gas and its temperature falls, an increasingly large fraction of the particles are forced into the lower energy states. If the gas particles are fermions, only one particle is allowed in each state; thus all the particles cannot crowd into the ground state. Instead, as the temperature of the gas is lowered, the fermions will fill up the lowest available unoccupied states, starting with the ground state, and then successively occupy the excited states with the lowest energy. Even in the limit  $T \rightarrow 0$  K, the vigorous motion of the fermions in excited states produces a pressure in the fermion gas. At zero temperature, *all* of the lower energy states and *none* of the higher energy states are occupied. Such a fermion gas is said to be completely **degenerate**.

#### The Fermi Energy

The maximum energy ( $\epsilon_F$ ) of any electron in a completely degenerate gas at  $T = 0$  K is known as the **Fermi energy**; see Fig. 16.5. To determine this limiting energy, imagine a three-dimensional box of length  $L$  on each side. Thinking of the electrons as being standing

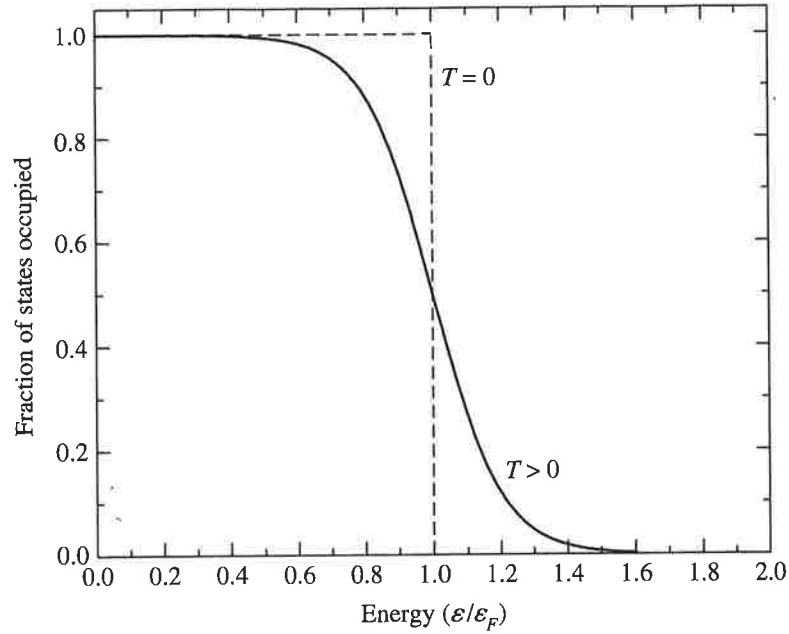


**FIGURE 16.5** Fraction of states of energy  $\varepsilon$  occupied by fermions. For  $T = 0$ , all fermions have  $\varepsilon \leq \varepsilon_F$ , but for  $T > 0$ , some fermions have energies in excess of the Fermi energy.

waves in the box, we note that their wavelengths in each dimension are given by

$$\lambda_x = \frac{2L}{N_x}, \quad \lambda_y = \frac{2L}{N_y}, \quad \lambda_z = \frac{2L}{N_z},$$

where  $N_x$ ,  $N_y$ , and  $N_z$  are integer quantum numbers associated with each dimension. Recalling that the de Broglie wavelength is related to momentum (Eq. 5.17),

$$p_x = \frac{hN_x}{2L}, \quad p_y = \frac{hN_y}{2L}, \quad p_z = \frac{hN_z}{2L}.$$

Now, the total kinetic energy of a particle can be written as

$$\varepsilon = \frac{p^2}{2m},$$

where  $p^2 = p_x^2 + p_y^2 + p_z^2$ . Thus,

$$\varepsilon = \frac{h^2}{8mL^2} (N_x^2 + N_y^2 + N_z^2) = \frac{h^2 N^2}{8mL^2}, \quad (16.2)$$

where  $N^2 \equiv N_x^2 + N_y^2 + N_z^2$ , analogous to the “distance” from the origin in “ $N$ -space” to the point  $(N_x, N_y, N_z)$ .

The total number of electrons in the gas corresponds to the total number of unique quantum numbers,  $N_x$ ,  $N_y$ , and  $N_z$  times two. The factor of two arises from the fact that electrons are spin  $\frac{1}{2}$  particles, so  $m_s = \pm 1/2$  implies that two electrons can have the same combination of  $N_x$ ,  $N_y$ , and  $N_z$  and still possess a unique set of *four* quantum numbers (including

spin). Now, each integer coordinate in  $N$ -space (e.g.,  $N_x = 1, N_y = 3, N_z = 1$ ) corresponds to the quantum state of two electrons. With a large enough sample of electrons, they can be thought of as occupying each integer coordinate out to a radius of  $N = \sqrt{N_x^2 + N_y^2 + N_z^2}$ , but only for the positive octant of  $N$ -space where  $N_x > 0, N_y > 0,$  and  $N_z > 0$ . This means that the total number of electrons will be

$$N_e = 2 \left( \frac{1}{8} \right) \left( \frac{4}{3} \pi N^3 \right).$$

Solving for  $N$  yields

$$N = \left( \frac{3N_e}{\pi} \right)^{1/3}.$$

Substituting into Eq. (16.2) and simplifying, we find that the Fermi energy is given by

$$\boxed{\varepsilon_F = \frac{\hbar^2}{2m} (3\pi^2 n)^{2/3}}, \quad (16.3)$$

where  $m$  is the mass of the electron and  $n \equiv N_e/L^3$  is the number of electrons per unit volume. The average energy per electron at zero temperature is  $\frac{3}{5}\varepsilon_F$ . (Of course the derivation above applies for any fermion, not just electrons.)

### The Condition for Degeneracy

At any temperature above absolute zero, some of the states with an energy less than  $\varepsilon_F$  will become vacant as fermions use their thermal energy to occupy other, more energetic states. Although the degeneracy will not be precisely complete when  $T > 0$  K, the assumption of complete degeneracy is a good approximation at the densities encountered in the interior of a white dwarf. All but the most energetic particles will have an energy less than the Fermi energy. To understand how the degree of degeneracy depends on both the temperature and the density of the white dwarf, we first express the Fermi energy in terms of the density of the electron gas. For full ionization, the number of electrons per unit volume is

$$n_e = \left( \frac{\# \text{ electrons}}{\text{nucleon}} \right) \left( \frac{\# \text{ nucleons}}{\text{volume}} \right) = \left( \frac{Z}{A} \right) \frac{\rho}{m_H}, \quad (16.4)$$

where  $Z$  and  $A$  are the number of protons and nucleons, respectively, in the white dwarf's nuclei, and  $m_H$  is the mass of a hydrogen atom.<sup>9</sup> Thus the Fermi energy is proportional to the  $2/3$  power of the density,

$$\varepsilon_F = \frac{\hbar^2}{2m_e} \left[ 3\pi^2 \left( \frac{Z}{A} \right) \frac{\rho}{m_H} \right]^{2/3}. \quad (16.5)$$

<sup>9</sup>The hydrogen mass is adopted as a representative mass of the proton and neutron.

Now compare the Fermi energy with the average thermal energy of an electron,  $\frac{3}{2}kT$  (where  $k$  is Boltzmann's constant; see Eq. 10.17). In rough terms, if  $\frac{3}{2}kT < \epsilon_F$ , then an average electron will be unable to make a transition to an unoccupied state, and the electron gas will be degenerate. That is, for a degenerate gas,

$$\frac{3}{2}kT < \frac{\hbar^2}{2m_e} \left[ 3\pi^2 \left( \frac{Z}{A} \right) \frac{\rho}{m_H} \right]^{2/3},$$

or

$$\frac{T}{\rho^{2/3}} < \frac{\hbar^2}{3m_e k} \left[ \frac{3\pi^2}{m_H} \left( \frac{Z}{A} \right) \right]^{2/3} = 1261 \text{ K m}^2 \text{ kg}^{-2/3}$$

for  $Z/A = 0.5$ . Defining

$$\mathcal{D} \equiv 1261 \text{ K m}^2 \text{ kg}^{-2/3},$$

the condition for degeneracy may be written as

$$\boxed{\frac{T}{\rho^{2/3}} < \mathcal{D}.} \quad (16.6)$$

The smaller the value of  $T/\rho^{2/3}$ , the more degenerate the gas.

---

**Example 16.3.1.** How important is electron degeneracy at the centers of the Sun and Sirius B? At the center of the standard solar model (see Table 11.1),  $T_c = 1.570 \times 10^7 \text{ K}$  and  $\rho_c = 1.527 \times 10^5 \text{ kg m}^{-3}$ . Then

$$\frac{T_c}{\rho_c^{2/3}} = 5500 \text{ K m}^2 \text{ kg}^{-2/3} > \mathcal{D}.$$

In the Sun, electron degeneracy is quite weak and plays a very minor role, supplying only a few tenths of a percent of the central pressure. However, as the Sun continues to evolve, electron degeneracy will become increasingly important (Fig. 16.6). As described in Section 13.2, the Sun will develop a degenerate helium core while on the red giant branch of the H-R diagram, leading eventually to a core helium flash. Later, on the asymptotic giant branch, the progenitor of a carbon-oxygen white dwarf will form in the core to be revealed when the Sun's surface layers are ejected as a planetary nebula.

For Sirius B, the values of the density and central temperature estimated above lead to

$$\frac{T_c}{\rho_c^{2/3}} = 37 \text{ K m}^2 \text{ kg}^{-2/3} \ll \mathcal{D},$$

so complete degeneracy is a valid assumption for Sirius B.

---

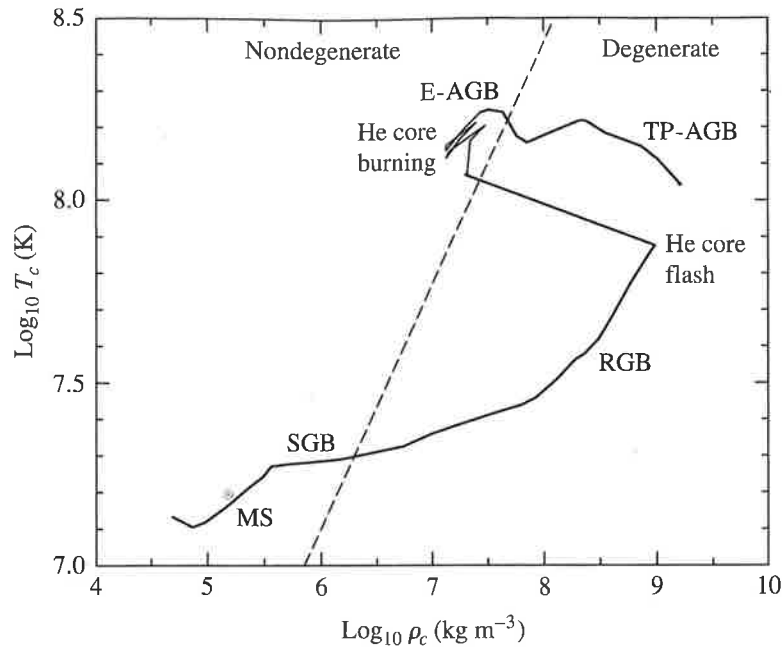


**FIGURE 16.6** Degeneracy in the Sun's center as it evolves. (Data from Mazzitelli and D'Antona, *Ap. J.*, 311, 762, 1986.)

### Electron Degeneracy Pressure

We now estimate the electron degeneracy pressure by combining two key ideas of quantum mechanics:

1. The Pauli exclusion principle, which allows at most one electron in each quantum state; and
2. Heisenberg's uncertainty principle in the form of Eq. (5.19),

$$\Delta x \Delta p_x \approx \hbar,$$

which requires that an electron confined to a small volume of space have a correspondingly high uncertainty in its momentum. Because the minimum value of the electron's momentum,  $p_{\min}$ , is approximately  $\Delta p$ , more closely confined electrons will have greater momenta.

When we make the unrealistic assumption that all of the electrons have the same momentum,  $p$ , Eq. (10.8) for the pressure integral becomes

$$P \approx \frac{1}{3} n_e p v, \quad (16.7)$$

where  $n_e$  is the total electron number density.

In a completely degenerate electron gas, the electrons are packed as tightly as possible, and for a uniform number density of  $n_e$ , the separation between neighboring electrons is

about  $n_e^{-1/3}$ . However, to satisfy the Pauli exclusion principle, the electrons must maintain their identities as different particles. That is, the uncertainty in their positions cannot be larger than their physical separation. Identifying  $\Delta x \approx n_e^{-1/3}$  for the limiting case of complete degeneracy, we can use Heisenberg's uncertainty relation to estimate the momentum of an electron. In one coordinate direction,

$$p_x \approx \Delta p_x \approx \frac{\hbar}{\Delta x} \approx \hbar n_e^{1/3} \quad (16.8)$$

(see Example 5.4.2). However, in a three-dimensional gas each of the directions is equally likely, implying that

$$p_x^2 = p_y^2 = p_z^2,$$

which is just a statement of the equipartition of energy among all the coordinate directions. Therefore,

$$p^2 = p_x^2 + p_y^2 + p_z^2 = 3p_x^2,$$

or

$$p = \sqrt{3} p_x.$$

Using Eq. (16.4) for the electron number density with full ionization gives

$$p \approx \sqrt{3} \hbar \left[ \left( \frac{Z}{A} \right) \frac{\rho}{m_H} \right]^{1/3}.$$

For nonrelativistic electrons, the speed is

$$\begin{aligned} v &= \frac{p}{m_e} \\ &\approx \frac{\sqrt{3} \hbar}{m_e} n_e^{1/3} \end{aligned} \quad (16.9)$$

$$\approx \frac{\sqrt{3} \hbar}{m_e} \left[ \left( \frac{Z}{A} \right) \frac{\rho}{m_H} \right]^{1/3}. \quad (16.10)$$

Inserting Eqs. (16.4), (16.8), and (16.10) into Eq. (16.7) for the electron degeneracy pressure results in

$$P \approx \frac{\hbar^2}{m_e} \left[ \left( \frac{Z}{A} \right) \frac{\rho}{m_H} \right]^{5/3}. \quad (16.11)$$

This is roughly a factor of two smaller than the exact expression for the pressure due to a completely degenerate, nonrelativistic electron gas  $P$ ,

$$P = \frac{(3\pi^2)^{2/3}}{5} \frac{\hbar^2}{m_e} n_e^{5/3},$$

or

$$P = \frac{(3\pi^2)^{2/3}}{5} \frac{\hbar^2}{m_e} \left[ \left( \frac{Z}{A} \right) \frac{\rho}{m_H} \right]^{5/3}. \quad (16.12)$$

Using  $Z/A = 0.5$  for a carbon–oxygen white dwarf, Eq. (16.12) shows that the electron degeneracy pressure available to support a white dwarf such as Sirius B is about  $1.9 \times 10^{22} \text{ N m}^{-2}$ , within a factor of two of the estimate of the central pressure made previously (Eq. 16.1). *Electron degeneracy pressure is responsible for maintaining hydrostatic equilibrium in a white dwarf.*

You may have noticed that Eq. (16.12) is the polytropic equation of state,  $P = K\rho^{5/3}$ , corresponding to  $n = 1.5$ . This implies that the extensive tools associated with the Lane–Emden equation (Eq. 10.110), developed beginning on page 334, can be used to study these objects. Of course, to understand them in detail requires careful numerical calculations involving the details of the complex equation of state of partially degenerate gases, nonzero temperatures, and changing compositions.

## 16.4 ■ THE CHANDRASEKHAR LIMIT

The requirement that degenerate electron pressure must support a white dwarf star has profound implications. In 1931, at the age of 21, the Indian physicist Subrahmanyan Chandrasekhar announced his discovery that *there is a maximum mass for white dwarfs*. In this section we will consider the physics that leads to this amazing conclusion.

### The Mass–Volume Relation

The relation between the radius,  $R_{\text{wd}}$ , of a white dwarf and its mass,  $M_{\text{wd}}$ , may be found by setting the estimate of the central pressure, Eq. (16.1), equal to the electron degeneracy pressure, Eq. (16.12):

$$\frac{2}{3} \pi G \rho^2 R_{\text{wd}}^2 = \frac{(3\pi^2)^{2/3}}{5} \frac{\hbar^2}{m_e} \left[ \left( \frac{Z}{A} \right) \frac{\rho}{m_H} \right]^{5/3}.$$

Using  $\rho = M_{\text{wd}} / \frac{4}{3} \pi R_{\text{wd}}^3$  (assuming constant density), this leads to an estimate of the radius of the white dwarf,

$$R_{\text{wd}} \approx \frac{(18\pi)^{2/3}}{10} \frac{\hbar^2}{G m_e M_{\text{wd}}^{1/3}} \left[ \left( \frac{Z}{A} \right) \frac{1}{m_H} \right]^{5/3}. \quad (16.13)$$

For a  $1 M_{\odot}$  carbon–oxygen white dwarf,  $R \approx 2.9 \times 10^6 \text{ m}$ , too small by roughly a factor of two but an acceptable estimate. More important is the surprising implication that  $M_{\text{wd}} R_{\text{wd}}^3 = \text{constant}$ , or

$$M_{\text{wd}} V_{\text{wd}} = \text{constant}. \quad (16.14)$$

The volume of a white dwarf is inversely proportional to its mass, so more massive white dwarfs are actually *smaller*. This **mass–volume relation** is a result of the star deriving its support from electron degeneracy pressure. The electrons must be more closely confined to generate the larger degeneracy pressure required to support a more massive star. In fact, the mass–volume relation implies that  $\rho \propto M_{\text{wd}}^2$ .

According to the mass–volume relation, piling more and more mass onto a white dwarf would eventually result in shrinking the star down to zero volume as its mass becomes infinite. However, if the density exceeds about  $10^9 \text{ kg m}^{-3}$ , there is a departure from this relation. To see why this is so, use Eq. (16.10) to estimate the speed of the electrons in Sirius B:

$$v \approx \frac{\hbar}{m_e} \left[ \left( \frac{Z}{A} \right) \frac{\rho}{m_H} \right]^{1/3} = 1.1 \times 10^8 \text{ m s}^{-1},$$

over one-third the speed of light! If the mass–volume relation were correct, white dwarfs a bit more massive than Sirius B would be so small and dense that their electrons would exceed the limiting value of the speed of light. This impossibility points out the dangers of ignoring the effects of relativity in our expressions for the electron speed (Eq. 16.10) and pressure (Eq. 16.11).<sup>10</sup> Because the electrons are moving more slowly than the nonrelativistic Eq. (16.10) would indicate, there is less electron pressure available to support the star. Thus a massive white dwarf is *smaller* than predicted by the mass–volume relation. Indeed, zero volume occurs for a finite value of the mass; in other words, there is a limit to the amount of matter that can be supported by electron degeneracy pressure.

### Dynamical Instability

To appreciate the effect of relativity on the stability of a white dwarf, recall that Eq. (16.12) (which is valid only for approximately  $\rho < 10^9 \text{ kg m}^{-3}$ ) is of the polytropic form  $P = K\rho^{5/3}$ , where  $K$  is a constant. Comparing this with Eq. (10.86) shows that the value of the ratio of specific heats is  $\gamma = 5/3$  in the nonrelativistic limit. As we discussed in Section 14.3, this means that the white dwarf is dynamically stable. If it suffers a small perturbation, it will return to its equilibrium structure instead of collapsing. However, in the extreme relativistic limit, the electron speed  $v = c$  must be used instead of Eq. (16.10) to find the electron degeneracy pressure. The result is

$$P = \frac{(3\pi^2)^{1/3}}{4} \hbar c \left[ \left( \frac{Z}{A} \right) \frac{\rho}{m_H} \right]^{4/3} \quad (16.15)$$

(see, for example, Problem 16.6). In this limit  $\gamma = 4/3$ , which corresponds to *dynamical instability*. The smallest departure from equilibrium will cause the white dwarf to collapse as electron degeneracy pressure fails.<sup>11</sup> As was explained in Section 15.3, approaching this

<sup>10</sup>It is left as an exercise to show that relativistic effects must be included for densities greater than  $10^9 \text{ kg m}^{-3}$ .

<sup>11</sup>In fact, the strong gravity of the white dwarf, as described by Einstein's general theory of relativity (see Section 17.1), acts to raise the critical value of  $\gamma$  for dynamical instability slightly above  $4/3$ .

limiting case leads to the collapse of the degenerate core in an aging supergiant, resulting in a core-collapse supernova. (Note that Eq. 16.15 is a polytropic equation of state,  $P = K\rho^{4/3}$ , with a polytropic index of  $n = 3$ .)

### Estimating the Chandrasekhar Limit

An approximate value for the maximum white-dwarf mass may be obtained by setting the estimate of the central pressure, Eq. (16.1) with  $\rho = M_{\text{wd}}/\frac{4}{3}\pi R_{\text{wd}}^3$ , equal to Eq. (16.15) with  $Z/A = 0.5$ . The radius of the white dwarf cancels, leaving

$$M_{\text{Ch}} \sim \frac{3\sqrt{2\pi}}{8} \left(\frac{\hbar c}{G}\right)^{3/2} \left[\left(\frac{Z}{A}\right) \frac{1}{m_H}\right]^2 = 0.44 M_{\odot} \quad (16.16)$$

for the greatest possible mass. Note that Eq. (16.16) contains three fundamental constants— $\hbar$ ,  $c$ , and  $G$ —representing the combined effects of quantum mechanics, relativity, and Newtonian gravitation on the structure of a white dwarf. A precise derivation with  $Z/A = 0.5$  results in a value of  $M_{\text{Ch}} = 1.44 M_{\odot}$ , called the **Chandrasekhar limit**. Figure 16.7 shows the mass–radius relation for white dwarfs.<sup>12</sup> No white dwarf has been discovered with a mass exceeding the Chandrasekhar limit.<sup>13</sup>

It is important to emphasize that neither the nonrelativistic nor the relativistic formula for the electron degeneracy pressure developed here (Eqs. 16.12 and 16.15, respectively) contains the temperature. Unlike the gas pressure of the ideal gas law and the expression for

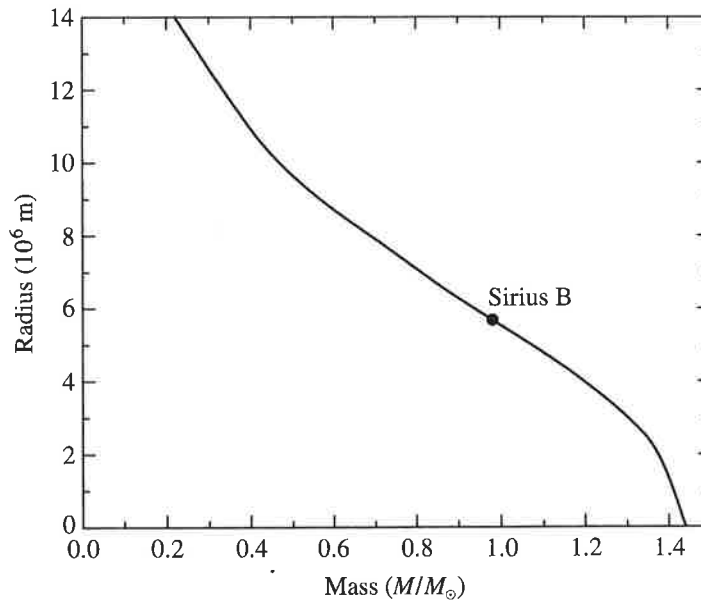


**FIGURE 16.7** Radii of white dwarfs of  $M_{\text{wd}} \leq M_{\text{Ch}}$  at  $T = 0$  K.

<sup>12</sup>Figure 16.7 does not include complications such as the electrostatic attraction between the nuclei and electrons in a white dwarf, thus tending to reduce the radius slightly.

<sup>13</sup>It is natural to wonder about the outcome of sneaking up on the Chandrasekhar limit by adding just a bit more mass to white dwarf with very nearly  $1.44 M_{\odot}$ . This will be considered in Section 18.5, where Type Ia supernovae are discussed.

radiation pressure, the pressure of a completely degenerate electron gas is independent of its temperature. This has the effect of decoupling the mechanical structure of the star from its thermal properties. However, the decoupling is never perfect since  $T > 0$ . As a result, the correct expression for the pressure involves treating the gas as partially degenerate and relativistic, but with  $v < c$ . This is a challenging equation of state to deal with properly.<sup>14</sup>

We have already seen one implication of this decoupling in Section 13.2, where the helium core flash was described as the result of the independence of the mechanical and thermal behavior of the degenerate helium core of a low-mass star. When helium burning begins in the core, it proceeds without an accompanying increase in pressure that would normally expand the core and therefore restrain the rising temperature. The resulting rapid rise in temperature leads to a runaway production of nuclear energy—the helium flash—which lasts until the temperature becomes sufficiently high to remove the degeneracy of the core, allowing it to expand. On the other hand, a star may have so little mass that its core temperature never becomes high enough to initiate helium burning. The result in this case is the formation of a helium white dwarf.

## 16.5 ■ THE COOLING OF WHITE DWARFS

Most stars end their lives as white dwarfs. These glowing embers scattered throughout space are a galaxy's memory of its past glory. Because no fusion occurs in their interiors, white dwarfs simply cool off at an essentially constant radius as they slowly deplete their supply of thermal energy (recall Fig. 16.3). Much effort has been directed at understanding the rate at which a white dwarf cools so its lifetime and the time of its birth may be calculated. Just as paleontologists can read the history of Earth's life in the fossil record, astronomers may be able to recover the history of star formation in our Galaxy by studying the statistics of white-dwarf temperatures. This section will be devoted to a discussion of the principles involved in this stellar archaeology.

### Energy Transport

First we must ask how energy is transported outward from the interior of a white dwarf. In an ordinary star, photons travel much farther than atoms do before suffering a collision that robs them of energy (recall Examples 9.2.1 and 9.2.2). As a result, photons are normally more efficient carriers of energy to the stellar surface. In a white dwarf, however, the degenerate electrons can travel long distances before losing energy in a collision with a nucleus, since the vast majority of the lower-energy electron states are already occupied. Thus, in a white dwarf, energy is carried by **electron conduction** rather than by radiation. This is so efficient that the interior of a white dwarf is nearly isothermal, with the temperature dropping significantly only in the nondegenerate surface layers. Figure 16.8 shows that a white dwarf consists of a nearly constant-temperature interior surrounded by a thin nondegenerate envelope that transfers heat less efficiently, causing the energy to leak out

<sup>14</sup>You are referred to Clayton (1983) or Hansen, Kawaler, and Trimble (2004) for a discussion of partial electron degeneracy.

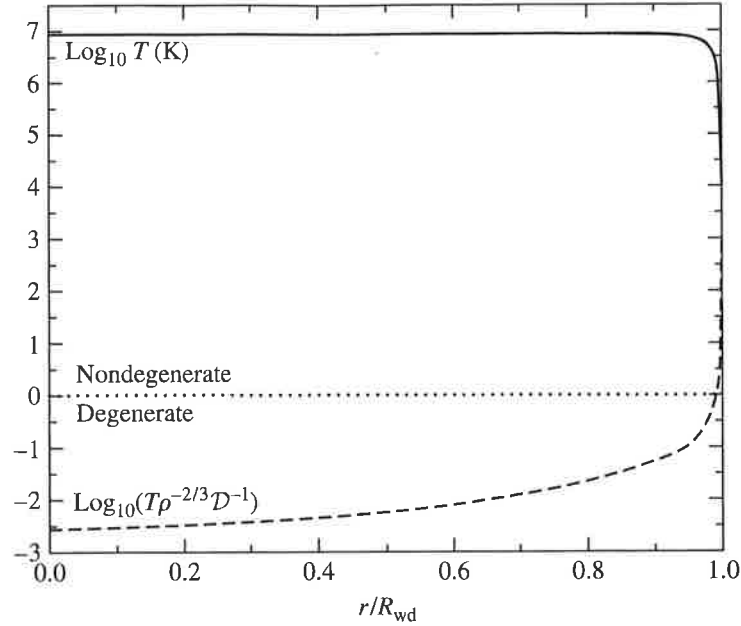


**FIGURE 16.8** Temperature and degree of degeneracy in the interior of a white dwarf model. The horizontal dotted line marks the boundary between degeneracy and nondegeneracy as described by Eq. (16.6).

slowly. The steep temperature gradient near the surface creates convection zones that may alter the appearance of the white dwarf's spectrum as it cools (as described in Section 16.2).

The structure of the nondegenerate surface layers of a star is described at the beginning of Appendix L. For a white dwarf of surface luminosity  $L_{\text{wd}}$  and mass  $M_{\text{wd}}$ , Eq. (L.1) for the pressure  $P$  as a function of the temperature  $T$  in the envelope is<sup>15</sup>

$$P = \left( \frac{4}{17} \frac{16\pi ac}{3} \frac{GM_{\text{wd}}}{L_{\text{wd}}} \frac{k}{\kappa_0 \mu m_H} \right)^{1/2} T^{17/4}, \quad (16.17)$$

where  $\kappa_0$  (called "A" in Eq. L.1) is the coefficient of the bound-free Kramers opacity law in Eq. (9.22),

$$\kappa_0 = 4.34 \times 10^{21} Z(1 + X) \text{ m}^2 \text{ kg}^{-1}.$$

Using the ideal gas law (Eq. 10.11) to replace the pressure results in a relation between the density and the temperature,

$$\rho = \left( \frac{4}{17} \frac{16\pi ac}{3} \frac{GM_{\text{wd}}}{L_{\text{wd}}} \frac{\mu m_H}{\kappa_0 k} \right)^{1/2} T^{13/4}. \quad (16.18)$$

The transition between the nondegenerate surface layers of the star and its isothermal, degenerate interior of temperature  $T_c$  is described by setting the two sides of Eq. (16.6) equal

<sup>15</sup>Equation (16.17) assumes that the envelope is in radiative equilibrium, with the energy carried outward by photons. Even when convection occurs in the surface layers of a white dwarf, it is not expected to have a large effect on the cooling.

to each other. Using this to replace the density results in an expression for the luminosity at the white dwarf's surface in terms of its interior temperature,

$$\begin{aligned} L_{\text{wd}} &= \frac{4D^3}{17} \frac{16\pi ac}{3} \frac{Gm_H}{\kappa_0 k} \mu M_{\text{wd}} T_c^{7/2} \\ &= CT_c^{7/2}, \end{aligned} \quad (16.19)$$

where

$$\begin{aligned} C &\equiv \frac{4D^3}{17} \frac{16\pi ac}{3} \frac{Gm_H}{\kappa_0 k} \mu M_{\text{wd}} \\ &= 6.65 \times 10^{-3} \left( \frac{M_{\text{wd}}}{M_\odot} \right) \frac{\mu}{Z(1+X)}. \end{aligned}$$

Note that the luminosity is proportional to  $T_c^{7/2}$  (the *interior* temperature) and that it varies as the fourth power of the *effective* temperature according to the Stefan–Boltzmann law, Eq. (3.17). Thus the surface of a white dwarf cools more slowly than its isothermal interior as the star's thermal energy leaks into space.

---

**Example 16.5.1.** Equation (16.19) can be used to estimate the interior temperature of a  $1 M_\odot$  white dwarf with  $L_{\text{wd}} = 0.03 L_\odot$ . Arbitrarily assuming values of  $X = 0$ ,  $Y = 0.9$ ,  $Z = 0.1$  for the nondegenerate envelope (so  $\mu \simeq 1.4$ ) results in<sup>16</sup>

$$T_c = \left[ \frac{L_{\text{wd}}}{6.65 \times 10^{-3}} \left( \frac{M_\odot}{M_{\text{wd}}} \right) \frac{Z(1+X)}{\mu} \right]^{2/7} = 2.8 \times 10^7 \text{ K}.$$

Equating the two sides of the degeneracy condition, Eq. (16.6), shows that the density at the base of the nondegenerate envelope is about

$$\rho = \left( \frac{T_c}{D} \right)^{3/2} = 3.4 \times 10^6 \text{ kg m}^{-3}.$$

This result is several orders of magnitude less than the average density of a  $1 M_\odot$  white dwarf such as Sirius B and confirms that the envelope is indeed thin, contributing very little to the star's total mass.

---

### The Cooling Timescale

A white dwarf's thermal energy resides primarily in the kinetic energy of its nuclei; the degenerate electrons cannot give up a significant amount of energy because nearly all of the lower energy states are already occupied. If we assume for simplicity that the composition is uniform, then the total number of nuclei in the white dwarf is equal to the star's mass,  $M_{\text{wd}}$ ,

<sup>16</sup>Because the amount of hydrogen is quite small even in a DA white dwarf, this composition is a reasonable choice for both type DA and type DB.

divided by the mass of a nucleus,  $Am_H$ . Furthermore, since the average thermal energy of a nucleus is  $\frac{3}{2}kT$ , the thermal energy available for radiation is

$$U = \frac{M_{\text{wd}}}{Am_H} \frac{3}{2} kT_c. \quad (16.20)$$

If we use the value of  $T_c$  from Example 16.5.1 and  $A = 12$  for carbon, Eq. (16.20) gives approximately  $6.0 \times 10^{40}$  J. A crude estimate of the characteristic timescale for cooling,  $\tau_{\text{cool}}$ , can be obtained simply by dividing the thermal energy by the luminosity. Thus

$$\tau_{\text{cool}} = \frac{U}{L_{\text{wd}}} = \frac{3}{2} \frac{M_{\text{wd}} k}{Am_H C T_c^{5/2}}, \quad (16.21)$$

which is about  $5.2 \times 10^{15}$  s  $\approx$  170 million years. This is an underestimate, because the cooling timescale increases as  $T_c$  decreases. The more detailed calculation that follows shows that a white dwarf spends most of its life cooling slowly with a low temperature and luminosity.

### The Change in Luminosity with Time

The depletion of the internal energy provides the luminosity, so Eqs. (16.19) and (16.20) give

$$-\frac{dU}{dt} = L_{\text{wd}}$$

or

$$-\frac{d}{dt} \left( \frac{M_{\text{wd}}}{Am_H} \frac{3}{2} kT_c \right) = C T_c^{7/2}.$$

If the initial temperature of the interior is  $T_0$  when  $t = 0$ , then this expression may be integrated to obtain the core temperature as a function of time:

$$T_c(t) = T_0 \left( 1 + \frac{5}{3} \frac{Am_H C T_0^{5/2}}{M_{\text{wd}} k} t \right)^{-2/5} = T_0 \left( 1 + \frac{5}{2} \frac{t}{\tau_0} \right)^{-2/5}, \quad (16.22)$$

where  $\tau_0$  is the timescale for cooling at the initial temperature of  $T_0$ ; that is,  $\tau_0 = \tau_{\text{cool}}$  at time  $t_0$ . Inserting this into Eq. (16.19) shows that the luminosity of the white dwarf first declines sharply from its initial value of  $L_0 = C T_0^{7/2}$  and then dims much more gradually as time passes:

$$L_{\text{wd}} = L_0 \left( 1 + \frac{5}{3} \frac{Am_H C^{2/7} L_0^{5/7}}{M_{\text{wd}} k} t \right)^{-7/5} = L_0 \left( 1 + \frac{5}{2} \frac{t}{\tau_0} \right)^{-7/5}. \quad (16.23)$$

The solid line in Fig. 16.9 shows the decline in the luminosity of a pure carbon  $0.6 M_{\odot}$  white dwarf calculated from Eq. (16.23). The dashed line is a curve obtained for a sequence

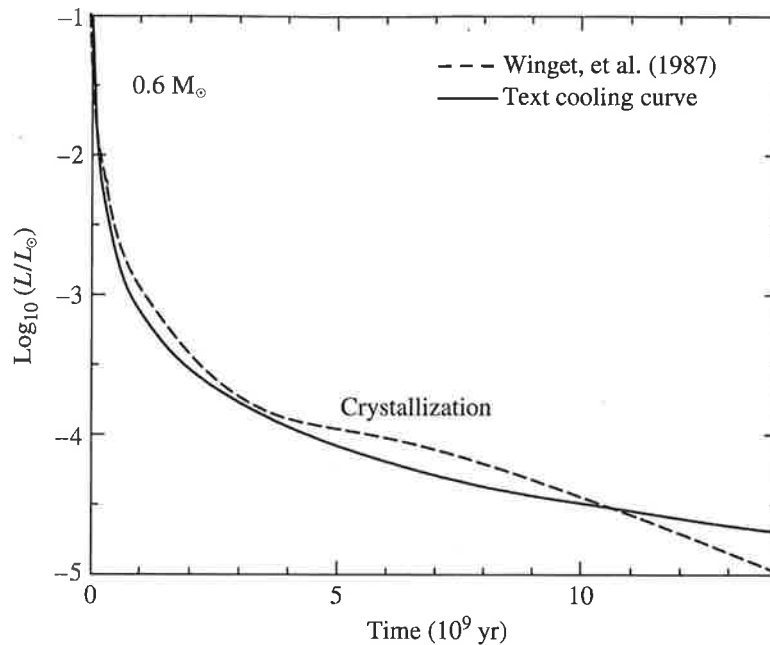


**FIGURE 16.9** Theoretical cooling curves for  $0.6 M_{\odot}$  white-dwarf models. [The solid line is from Eq. (16.23), and the dashed line is from Winget et al., *Ap. J. Lett.*, 315, L77, 1987.]

of more realistic white-dwarf models<sup>17</sup> that include thin surface layers of hydrogen and helium overlying the carbon core. The insulating effect of these layers slows the cooling by about 15%. Also included are some of the intriguing phenomena that occur as the white dwarf's internal temperature drops.

### Crystallization

As a white dwarf cools, it crystallizes in a gradual process that starts at the center and moves outward. The upturned “knee” in the dashed curve in Fig. 16.9 at about  $L_{wd}/L_{\odot} \approx 10^{-4}$  occurs when the cooling nuclei begin settling into a crystalline lattice. The regular crystal structure is maintained by the mutual electrostatic repulsion of the nuclei; it minimizes their energy as they vibrate about their average position in the lattice. As the nuclei undergo this phase change, they release their latent heat (about  $kT$  per nucleus), slowing the star's cooling and producing the knee in the cooling curve. Later, as the white dwarf's temperature continues to drop, the crystalline lattice actually accelerates the cooling as the coherent vibration of the regularly spaced nuclei promotes further energy loss. This is reflected in the subsequent downturn in the cooling curve. Thus the ultimate monument to the lives of most stars will be a “diamond in the sky,” a cold, dark, Earth-size sphere of crystallized carbon and oxygen floating through the depths of space.<sup>18</sup>

<sup>17</sup>You are referred to Winget et al. (1987) for details of this and other cooling curves.

<sup>18</sup>Unlike a terrestrial diamond, the white dwarf's nuclei are arrayed in a body-centered cubic lattice like that of metallic sodium.

### Comparing Theory with Observations

Despite the large uncertainties in the measurement of surface temperatures resulting from high surface gravities and broad spectral features,<sup>19</sup> it is possible to observe the cooling of a pulsating white dwarf. As the star's temperature declines, its period  $P$  slowly changes according to  $dP/dt \propto T^{-1}$  (approximately). Extremely precise measurements of a rapidly cooling DOV star yield a period derivative of  $P/|dP/dt| = 1.4 \times 10^6$  years, in excellent agreement with the theoretical value. Measuring period changes for the more slowly cooling DBV and DAV stars are even more difficult.

This interest in an accurate calculation of the decline in a white dwarf's temperature reflects the hope of using these fossil stars as a tool for uncovering the history of star formation in our Galaxy. Figure 16.10, from Winget et al. (1987), illustrates how this might be accomplished. Each circle (both open and filled) in the figure is the observed number of white dwarfs per cubic parsec with the absolute visual magnitude given at the top of the figure. The dramatically sudden drop in the population of white dwarfs with  $L_{\text{wd}}/L_{\odot} < -4.5$  is inconsistent with the assumption that stars have been forming in our Galaxy throughout the infinite past. Instead, this decline can best be explained if the first white dwarfs were formed and began cooling 9.0  $\pm$  1.8 billion years ago. Figure 16.10 shows the theoretically expected distribution of white dwarf luminosities based on this cooling time, calculated using theoretical cooling curves similar to the one shown in Fig. 16.9

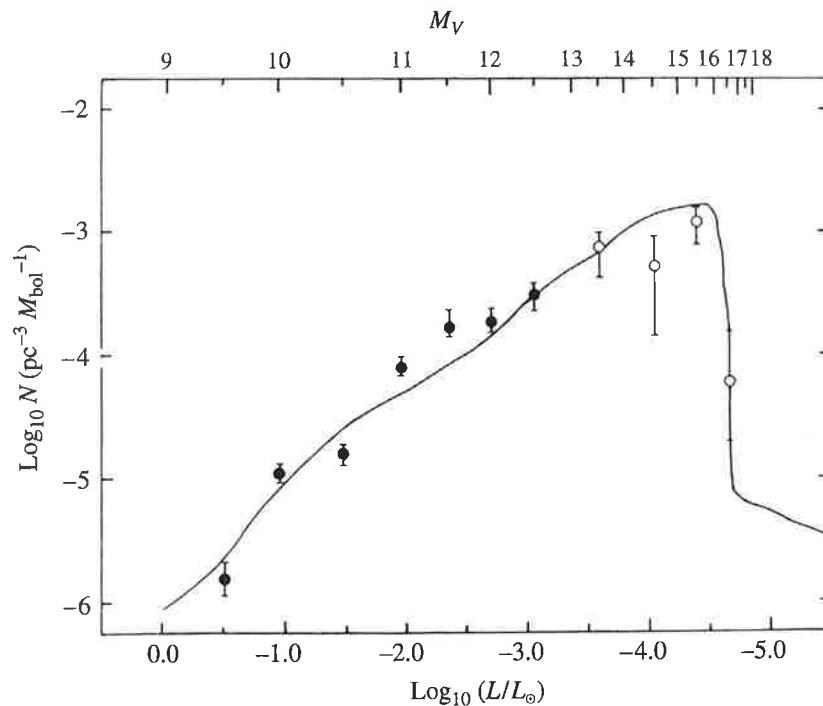


**FIGURE 16.10** Observed and theoretical distribution of white-dwarf luminosities. (Figure adapted from Winget et al., *Ap. J. Lett.*, 315, L77, 1987.)

<sup>19</sup>For Sirius B, effective temperatures ranging from 27,000 K to 32,000 K are often quoted.

together with the observed distribution of white-dwarf masses. Furthermore, adding the time spent in the pre-white-dwarf stages of stellar evolution implies that star formation in the disk of our Galaxy began about  $9.3 \pm 2.0$  billion years ago.<sup>20</sup> This time is about 3 billion years shorter than the age determined for the Milky Way's globular clusters, which formed at an earlier epoch.

## 16.6 ■ NEUTRON STARS

Two years after James Chadwick (1891–1974) discovered the neutron in 1932, a German astronomer and a Swiss astrophysicist, Walter Baade (1893–1960) and Fritz Zwicky (1898–1974) of Mount Wilson Observatory, proposed the existence of **neutron stars**. These two astronomers, who also coined the term *supernova*, went on to suggest that “supernovae represent the transitions from ordinary stars into neutron stars, which in their final stages consist of extremely closely packed neutrons.”

### Neutron Degeneracy

Because neutron stars are formed when the degenerate core of an aging supergiant star nears the Chandrasekhar limit and collapses, we take  $M_{\text{Ch}}$  (rounded to two figures) for a typical neutron star mass. A 1.4-solar-mass neutron star would consist of  $1.4 M_{\odot}/m_n \approx 10^{57}$  neutrons—in effect, a huge nucleus with a mass number of  $A \approx 10^{57}$  that is held together by gravity and supported by **neutron degeneracy pressure**.<sup>21</sup> It is left as an exercise to show that

$$R_{\text{ns}} \approx \frac{(18\pi)^{2/3}}{10} \frac{\hbar^2}{GM_{\text{ns}}^{1/3}} \left( \frac{1}{m_H} \right)^{8/3} \quad (16.24)$$

is the expression for the estimated neutron star radius, analogous to Eq. (16.13) for a white dwarf. For  $M_{\text{ns}} = 1.4 M_{\odot}$ , this yields a value of 4400 m. As we found with Eq. (16.13) for white dwarfs, this estimate is too small by a factor of about 3. That is, the actual radius of a  $1.4 M_{\odot}$  neutron star lies roughly between 10 and 15 km; we will adopt a value of 10 km for the radius. As will be seen, there are many uncertainties involved in the construction of a model neutron star.

### The Density of a Neutron Star

This incredibly compact stellar remnant would have an average density of  $6.65 \times 10^{17} \text{ kg m}^{-3}$ , greater than the typical density of an atomic nucleus,  $\rho_{\text{nuc}} \approx 2.3 \times 10^{17} \text{ kg m}^{-3}$ . In some sense, the neutrons in a neutron star must be “touching” one another. At the density of a neutron star, all of Earth's human inhabitants could be crowded into a cube 1.5 cm on each side.<sup>22</sup>

<sup>20</sup>Other, more recent studies have obtained similar results for the age of the *thin disk* of our Galaxy based on white-dwarf cooling times; age estimates range from 9 Gyr to 11 Gyr.

<sup>21</sup>Like electrons, neutrons are fermions and so are subject to the Pauli exclusion principle.

<sup>22</sup>Astronomer Frank Shu has commented that this shows “how much of humanity is empty space”!

The pull of gravity at the surface of a neutron star is fierce. For a  $1.4 M_{\odot}$  neutron star with a radius of 10 km,  $g = 1.86 \times 10^{12} \text{ m s}^{-2}$ , 190 billion times stronger than the acceleration of gravity at Earth's surface. An object dropped from a height of one meter would arrive at the star's surface with a speed of  $1.93 \times 10^6 \text{ m s}^{-1}$  (about 4.3 million mph).

---

**Example 16.6.1.** The inadequacy of using Newtonian mechanics to describe neutron stars can be demonstrated by calculating the escape velocity at the surface. Using Eq. (2.17), we find

$$v_{\text{esc}} = \sqrt{2GM_{\text{ns}}/R_{\text{ns}}} = 1.93 \times 10^6 \text{ m s}^{-1} = 0.643c.$$

This can also be seen by considering the ratio of the Newtonian gravitational potential energy to the rest energy of an object of mass  $m$  at the star's surface:

$$\frac{GM_{\text{ns}}m/R_{\text{ns}}}{mc^2} = 0.207.$$

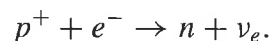
Clearly, the effects of relativity must be included for an accurate description of a neutron star. This applies not only to Einstein's theory of special relativity, described in Chapter 4, but also to his theory of gravity, called the *general theory of relativity*, which will be considered in Section 17.1. Nevertheless, we will use both relativistic formulas and the more familiar Newtonian physics to reach qualitatively correct conclusions about neutron stars.

---

### The Equation of State

To appreciate the exotic nature of the material constituting a neutron star and the difficulties involved in calculating the equation of state, imagine compressing the mixture of iron nuclei and degenerate electrons that make up an iron white dwarf at the center of a massive supergiant star.<sup>23</sup> Specifically, we are interested in the equilibrium configuration of  $10^{57}$  nucleons (protons and neutrons), together with enough free electrons to provide zero net charge. The equilibrium arrangement is the one that involves the least energy.

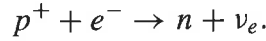
Initially, at low densities the nucleons are found in iron nuclei. This is the outcome of the minimum-energy compromise between the repulsive Coulomb force between the protons and the attractive nuclear force between all of the nucleons. However, as mentioned in the discussion of the Chandrasekhar limit (Section 16.4), when  $\rho \approx 10^9 \text{ kg m}^{-3}$  the electrons become relativistic. Soon thereafter, the minimum-energy arrangement of protons and neutrons changes because the energetic electrons can convert protons in the iron nuclei into neutrons by the process of electron capture (Eq. 15.6),



Because the neutron mass is slightly greater than the sum of the proton and electron masses, and the neutrino's rest-mass energy is negligible, the electron must supply the kinetic energy to make up the difference in energy;  $m_n c^2 - m_p c^2 - m_e c^2 = 0.78 \text{ MeV}$ .

<sup>23</sup>Because the mechanical and thermal properties of degenerate matter are independent of one another, we will assume for convenience that  $T = 0 \text{ K}$ . The iron nuclei are then arranged in a crystalline lattice.

**Example 16.6.2.** We will obtain an estimate of the density at which the process of electron capture begins for a simple mixture of hydrogen nuclei (protons) and relativistic degenerate electrons,



In the limiting case when the neutrino carries away no energy, we can equate the relativistic expression for the electron kinetic energy, Eq. (4.45), to the difference between the neutron rest energy and combined proton and electron rest energies and write

$$m_e c^2 \left( \frac{1}{\sqrt{1 - v^2/c^2}} - 1 \right) = (m_n - m_p - m_e) c^2,$$

or

$$\left( \frac{m_e}{m_n - m_p} \right)^2 = 1 - \frac{v^2}{c^2}.$$

Although Eq. (16.10) for the electron speed is strictly valid only for nonrelativistic electrons, it is accurate enough to be used in this estimate. Inserting this expression for  $v$  leads to

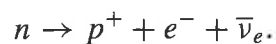
$$\left( \frac{m_e}{m_n - m_p} \right)^2 \approx 1 - \frac{\hbar^2}{m_e^2 c^2} \left[ \left( \frac{Z}{A} \right) \frac{\rho}{m_H} \right]^{2/3}.$$

Solving for  $\rho$  shows that the density at which electron capture begins is approximately

$$\rho \approx \frac{A m_H}{Z} \left( \frac{m_e c}{\hbar} \right)^3 \left[ 1 - \left( \frac{m_e}{m_n - m_p} \right)^2 \right]^{3/2} \approx 2.3 \times 10^{10} \text{ kg m}^{-3},$$

using  $A/Z = 1$  for hydrogen. This is in reasonable agreement with the actual value of  $\rho = 1.2 \times 10^{10} \text{ kg m}^{-3}$ .

We considered free protons in Example 16.6.2 to avoid the complications that arise when they are bound in heavy nuclei. A careful calculation that takes into account the surrounding nuclei and relativistic degenerate electrons, as well as the complexities of nuclear physics, reveals that the density must exceed  $10^{12} \text{ kg m}^{-3}$  for the protons in  ${}^{56}_{26}\text{Fe}$  nuclei to capture electrons. At still higher densities, the most stable arrangement of nucleons is one where the neutrons and protons are found in a lattice of increasingly neutron-rich nuclei so as to decrease the energy due to the Coulomb repulsion between protons. This process is known as **neutronization** and produces a sequence of nuclei such as  ${}^{56}_{26}\text{Fe}$ ,  ${}^{62}_{28}\text{Ni}$ ,  ${}^{64}_{28}\text{Ni}$ ,  ${}^{66}_{28}\text{Ni}$ ,  ${}^{86}_{36}\text{Kr}$ ,  $\dots$ ,  ${}^{118}_{36}\text{Kr}$ . Ordinarily, these supernumerary neutrons would revert to protons via the standard  $\beta$ -decay process,



However, under the conditions of complete electron degeneracy, there are no vacant states available for an emitted electron to occupy, so the neutrons cannot decay back into protons.<sup>24</sup>

When the density reaches about  $4 \times 10^{14} \text{ kg m}^{-3}$ , the minimum-energy arrangement is one in which some of the neutrons are found *outside* the nuclei. The appearance of these free neutrons is called **neutron drip** and marks the start of a three-component mixture of a lattice of neutron-rich nuclei, nonrelativistic degenerate free neutrons, and relativistic degenerate electrons.

The fluid of free neutrons has the striking property that it has no viscosity. This occurs because a spontaneous pairing of the degenerate neutrons has taken place. The resulting combination of two fermions (the neutrons) is a boson (recall Section 5.4) and so is not subject to the restrictions of the Pauli exclusion principle. Because degenerate bosons can *all* crowd into the lowest energy state, the fluid of paired neutrons can lose no energy. It is a **superfluid** that flows without resistance. Any whirlpools or vortices in the fluid will continue to spin forever without stopping.

As the density increases further, the number of free neutrons increases as the number of electrons declines. The neutron degeneracy pressure exceeds the electron degeneracy pressure when the density reaches roughly  $4 \times 10^{15} \text{ kg m}^{-3}$ . As the density approaches  $\rho_{\text{nuc}}$ , the nuclei effectively dissolve as the distinction between neutrons inside and outside of nuclei becomes meaningless. This results in a fluid mixture of free neutrons, protons, and electrons dominated by neutron degeneracy pressure, with both the neutrons and protons paired to form superfluids. The fluid of pairs of positively charged protons is also **superconducting**, with zero electrical resistance. As the density increases further, the ratio of neutrons:protons:electrons approaches a limiting value of 8:1:1, as determined by the balance between the competing processes of electron capture and  $\beta$ -decay inhibited by the presence of degenerate electrons.

The properties of the neutron star material when  $\rho > \rho_{\text{nuc}}$  are still poorly understood. A complete theoretical description of the behavior of a sea of free neutrons interacting via the strong nuclear force in the presence of protons and electrons is not yet available, and there is little experimental data on the behavior of matter in this density range. A further complication is the appearance of sub-nuclear particles such as *pions* ( $\pi$ ) produced by the decay of a neutron into a proton and a negatively charged pion,  $n \rightarrow p^+ + \pi^-$ , which occurs spontaneously in neutron stars when  $\rho > 2\rho_{\text{nuc}}$ .<sup>25</sup> Nevertheless, these are the values of the density encountered in the interiors of neutron stars, and the difficulties mentioned are the primary reasons for the uncertainty in the structure calculated for model neutron stars.

### Neutron Star Models

Table 16.1 summarizes the composition of the neutron star material at various densities. After an equation of state that relates the density and pressure has been obtained, a model of the star can be calculated by numerically integrating general-relativistic versions of the

<sup>24</sup>An *isolated* neutron decays into a proton in about 10.2 minutes, the half-life for that process.

<sup>25</sup>The  $\pi^-$  is a negatively charged particle that is 273 times more massive than the electron. It mediates the strong nuclear force that holds an atomic nucleus together. (The strong force between nucleons was described in Section 10.3.) Pions have been produced and studied in high-energy accelerator laboratories.

**TABLE 16.1** Composition of Neutron Star Material.

Transition density ( $\text{kg m}^{-3}$ )	Composition	Degeneracy pressure
$\approx 1 \times 10^9$	iron nuclei, nonrelativistic free electrons	electron
	electrons become relativistic	
$\approx 1 \times 10^{12}$	iron nuclei, relativistic free electrons	electron
	neutronization	
$\approx 4 \times 10^{14}$	neutron-rich nuclei, relativistic free electrons	electron
	neutron drip	
$\approx 4 \times 10^{15}$	neutron-rich nuclei, free neutrons, relativistic free electrons	electron
	neutron degeneracy pressure dominates	
$\approx 2 \times 10^{17}$	neutron-rich nuclei, superfluid free neutrons, relativistic free electrons	neutron
	nuclei dissolve	
$\approx 4 \times 10^{17}$	superfluid free neutrons, superconducting free protons, relativistic free electrons	neutron
	pion production	
	superfluid free neutrons, superconducting free protons, relativistic free electrons, other elementary particles (pions, ...?)	neutron

stellar structure equations collected at the beginning of Section 10.5. The first quantitative model of a neutron star was calculated by J. Robert Oppenheimer (1904–1967) and G. M. Volkoff (1914–2000) at Berkeley in 1939. Figure 16.11 shows the result of a recent calculation of a  $1.4 M_{\odot}$  neutron star model. Although the details are sensitive to the equation of state used, this model displays some typical features.

1. The outer crust consists of heavy nuclei, in the form of either a fluid “ocean” or a solid lattice, and relativistic degenerate electrons. Nearest the surface, the nuclei are probably  ${}^{56}_{26}\text{Fe}$ . At greater depth and density, increasingly neutron-rich nuclei are encountered until neutron drip begins at the bottom of the outer crust (where  $\rho \approx 4 \times 10^{14} \text{ kg m}^{-3}$ ).
2. The inner crust consists of a three-part mixture of a lattice of nuclei such as  ${}^{118}_{36}\text{Kr}$ , a superfluid of free neutrons, and relativistic degenerate electrons. The bottom of the inner crust occurs where  $\rho \approx \rho_{\text{nuc}}$ , and the nuclei dissolve.

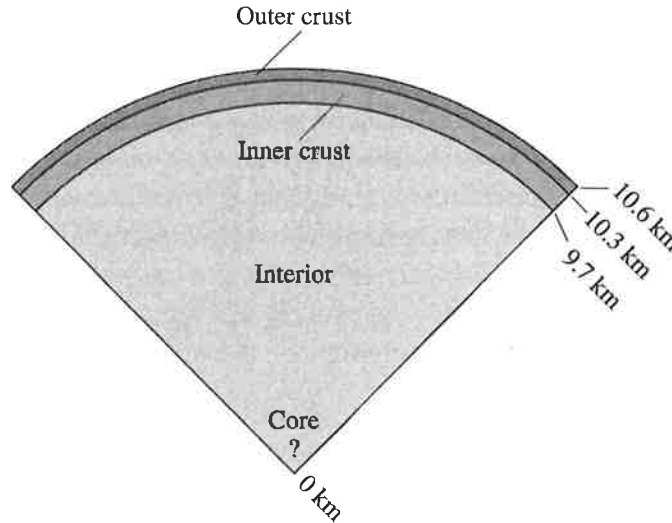


FIGURE 16.11 A  $1.4 M_{\odot}$  neutron star model.

3. The interior of the neutron star consists primarily of superfluid neutrons, with a smaller number of superfluid, superconducting protons and relativistic degenerate electrons.
4. There may or may not be a solid core consisting of pions or other sub-nuclear particles. The density at the center of a  $1.4 M_{\odot}$  neutron star is about  $10^{18} \text{ kg m}^{-3}$ .

### The Chandrasekhar Limit for Neutron Stars

Like white dwarfs, neutron stars obey a mass–volume relation,

$$M_{\text{ns}} V_{\text{ns}} = \text{constant}, \quad (16.25)$$

so neutron stars become smaller and more dense with increasing mass. However, this mass–volume relation fails for more massive neutron stars because there is a point beyond which neutron degeneracy pressure can no longer support the star. Hence, there is a maximum mass for neutron stars, analogous to the Chandrasekhar mass for white dwarfs. As might be expected, the value of this maximum mass is different for different choices of the equation of state. However, detailed computer modeling of neutron stars, along with a very general argument involving the general theory of relativity, shows that the maximum mass possible for a neutron star cannot exceed about  $2.2 M_{\odot}$  if it is static, and  $2.9 M_{\odot}$  if it is rotating rapidly.<sup>26</sup> If a neutron star is to remain dynamically stable and resist collapsing, it must be able to respond to a small disturbance in its structure by rapidly adjusting its pressure to compensate. However, there is a limit to how quickly such an adjustment can be made because these changes are conveyed by sound waves that must move more slowly than light. If a neutron star's mass exceeds  $2.2 M_{\odot}$  in the static case or  $2.9 M_{\odot}$  in the rapidly rotating case, it cannot generate pressure quickly enough to avoid collapsing. The result is a black hole (as will be discussed in Section 17.3).

<sup>26</sup>Recall from Section 15.4 that centrifugal effects provide additional support to a rapidly rotating neutron star.

### Rapid Rotation and Conservation of Angular Momentum

Several properties of neutron stars were anticipated before they were observed. For example, neutron stars must rotate very rapidly. If the iron core of the pre-supernova supergiant star were rotating even slowly, the decrease in radius would be so great that the conservation of angular momentum would guarantee the formation of a rapidly rotating neutron star.

The scale of the collapse can be found from Eqs. (16.13) and (16.24) for the estimated radii of a white dwarf and neutron star if we assume that the progenitor core is characteristic of a white dwarf composed entirely of iron. Although the leading constants in both expressions are spurious (a by-product of the approximations made), the *ratio* of the radii is more accurate:

$$\frac{R_{\text{core}}}{R_{\text{ns}}} \approx \frac{m_n}{m_e} \left( \frac{Z}{A} \right)^{5/3} = 512,$$

where  $Z/A = 26/56$  for iron has been used. Now apply the conservation of angular momentum to the collapsing core (which is assumed here for simplicity to lose no mass, so  $M_{\text{core}} = M_{\text{wd}} = M_{\text{ns}}$ ). Treating each star as a sphere with a moment of inertia of the form  $I = CMR^2$ , we have<sup>27</sup>

$$\begin{aligned} I_i \omega_i &= I_f \omega_f \\ CM_i R_i^2 \omega_i &= CM_f R_f^2 \omega_f \\ \omega_f &= \omega_i \left( \frac{R_i}{R_f} \right)^2. \end{aligned}$$

In terms of the rotation period  $P$ , this is

$$P_f = P_i \left( \frac{R_f}{R_i} \right)^2. \quad (16.26)$$

For the specific case of an iron core collapsing to form a neutron star, Eq. (16.6) shows that

$$P_{\text{ns}} \approx 3.8 \times 10^{-6} P_{\text{core}}. \quad (16.27)$$

The question of how fast the progenitor core may be rotating is difficult to answer. As a star evolves, its contracting core is not completely isolated from the surrounding envelope, so one cannot use the simple approach to conservation of angular momentum described above.<sup>28</sup> For purposes of estimation, we will take  $P_{\text{core}} = 1350$  s, the rotation period observed for the white dwarf 40 Eridani B (shown in the H-R diagrams of Figs. 8.12 and 8.16). Inserting this into Eq. (16.27) results in a rotation period of about  $5 \times 10^{-3}$  s. Thus neutron stars will be rotating very rapidly when they are formed, with rotation periods on the order of a few milliseconds.

<sup>27</sup>The constant  $C$  is determined by the distribution of mass inside the star. For example,  $C = 2/5$  for a uniform sphere. We assume that the progenitor core and neutron star have about the same value of  $C$ .

<sup>28</sup>The core and envelope may exchange angular momentum by magnetic fields or rotational mixing via the very slow *meridional currents* that generally circulate upward at the poles and downward at the equator of a rotating star.

### “Freezing In” Magnetic Field Lines

Another property predicted for neutron stars is that they should have extremely strong magnetic fields. The “freezing in” of magnetic field lines in a conducting fluid or gas (mentioned in Section 11.3 in connection with sunspots) implies that the *magnetic flux* through the surface of a white dwarf will be conserved as it collapses to form a neutron star. The flux of a magnetic field through a surface  $S$  is defined as the surface integral

$$\Phi \equiv \int_S \mathbf{B} \cdot d\mathbf{A},$$

where  $\mathbf{B}$  is the magnetic field vector (see Fig. 16.12). In approximate terms, if we ignore the geometry of the magnetic field, this means that the product of the magnetic field strength and the area of the star’s surface remains constant. Thus

$$B_i 4\pi R_i^2 = B_f 4\pi R_f^2. \quad (16.28)$$

In order to use Eq. (16.28) to estimate the magnetic field of a neutron star, we must first know what the strength of the magnetic field is for the iron core of a pre-supernova star. Although this is not at all clear, we can use the largest observed white-dwarf magnetic field of  $B \approx 5 \times 10^4$  T as an extreme case, which is large compared to a typical white-dwarf magnetic field of perhaps 10 T, and huge compared with the Sun’s global field of about  $2 \times 10^{-4}$  T. Then, using Eq. (16.6), the magnetic field of the neutron star would be

$$B_{\text{ns}} \approx B_{\text{wd}} \left( \frac{R_{\text{wd}}}{R_{\text{ns}}} \right)^2 = 1.3 \times 10^{10} \text{ T}.$$

This shows that neutron stars could be formed with extremely strong magnetic fields, although smaller values such as  $10^8$  T or less are more typical.

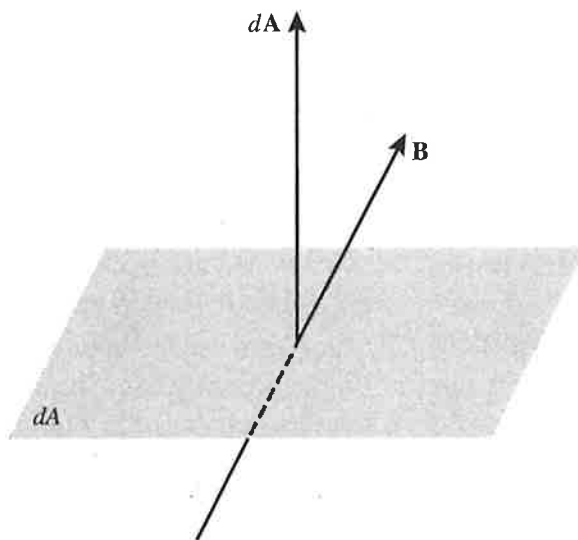
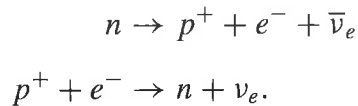


FIGURE 16.12 Magnetic flux,  $d\Phi = \mathbf{B} \cdot d\mathbf{A}$ , through an element of surface area  $dA$ .

### Neutron Star Temperatures

The final property of neutron stars is the most obvious. They were extremely hot when they were forged in the “fires” of a supernova, with  $T \sim 10^{11}$  K. During the first day, the neutron star cools by emitting neutrinos via the so-called **URCA process**,<sup>29</sup>



As the nucleons shuttle between being neutrons and being protons, large numbers of neutrinos and antineutrinos are produced that fly unhindered into space, carrying away energy and thus cooling the neutron star. This process can continue only as long as the nucleons are not degenerate, and it is suppressed after the protons and neutrons settle into the lowest unoccupied energy states. This degeneracy occurs about one day after the formation of the neutron star, when its internal temperature has dropped to about  $10^9$  K. Other neutrino-emitting processes continue to dominate the cooling for approximately the first thousand years, after which photons emitted from the star’s surface take over. The neutron star is a few hundred years old when its internal temperature has declined to  $10^8$  K, with a surface temperature of several million K. By now the cooling has slowed considerably, and the surface temperature will hover around  $10^6$  K for the next ten thousand years or so as the neutron star cools at an essentially constant radius.

It is interesting to calculate the blackbody luminosity of a  $1.4 M_\odot$  neutron star with a surface temperature of  $T = 10^6$  K. From the Stefan–Boltzmann law, Eq. (3.17),

$$L = 4\pi R^2 \sigma T_e^4 = 7.13 \times 10^{25} \text{ W.}$$

Although this is comparable to the luminosity of the Sun, the radiation is primarily in the form of X-rays since, according to Wien’s displacement law, Eq. (3.19),

$$\lambda_{\text{max}} = \frac{(500 \text{ nm})(5800 \text{ K})}{T} = 2.9 \text{ nm.}$$

Prior to the advent of X-ray observatories such as ROSAT, ASCA, and Chandra, astronomers held little hope of ever observing such an exotic object, barely the size of San Diego, California.

## 16.7 ■ PULSARS

Jocelyn Bell spent two years setting up a forest of 2048 radio dipole antennae over four and a half acres of English countryside. She and her Ph.D. thesis advisor, Anthony Hewish, were using this radio telescope, tuned to a frequency of 81.5 MHz, to study the scintillation (“flickering”) that is observed when the radio waves from distant sources known as quasars

<sup>29</sup>The URCA process, which efficiently removes energy from a hot neutron star, is named for the Casino de URCA in Rio de Janeiro, in remembrance of the efficiency with which it removed money from an unlucky physicist. The casino was closed by Brazil in 1955.

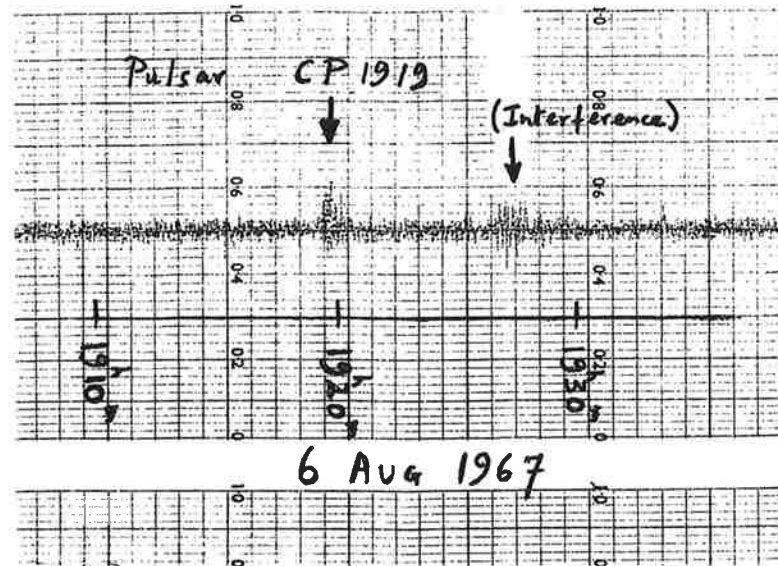


**FIGURE 16.13** Discovery of the first pulsar, PSR 1919+21 (“CP” stands for Cambridge Pulsar). (Figure from Lyne and Graham-Smith, *Pulsar Astronomy*, ©Cambridge University Press, New York, 1990. Reprinted with the permission of Cambridge University Press.)

pass through the solar wind. In July 1967, Bell was puzzled to find a bit of “scruff” that reappeared every 400 feet or so on the rolls of her strip chart recorder; see Fig. 16.13. Careful measurements showed that this quarter inch of ink reappeared every 23 hours and 56 minutes, indicating that its source passed over her fixed array of antennae once every sidereal day. Bell concluded that the source was out among the stars rather than within the Solar System. To better resolve the signal, she used a faster recorder and discovered that the scruff consisted of a series of regularly spaced radio pulses 1.337 s apart (the pulse period,  $P$ ). Such a precise celestial clock was unheard of, and Bell and Hewish considered the possibility that these might be signals from an extraterrestrial civilization. If this were true, she felt annoyed that the aliens had chosen such an inconvenient time to make contact. She recalled, “I was now two and a half years through a three year studentship and here was some silly lot of Little Green Men using *my* telescope and *my* frequency to signal to planet Earth.” When Bell found another bit of scruff, coming from another part of the sky, her relief was palpable. She wrote, “It was highly unlikely that two lots of Little Green Men could choose the same unusual frequency and unlikely technique to signal to the same inconspicuous planet Earth!”

Hewish, Bell, and their colleagues announced the discovery of these mysterious **pulsars**,<sup>30</sup> and several more were quickly found by other radio observatories. At the time this text was written, more than 1500 pulsars were known, and each is designated by a “PSR”

<sup>30</sup>The term *pulsar* was coined by the science correspondent for the London *Daily Telegraph*. See Hewish et al. (1968) for details of the discovery of pulsars. In 1974 Hewish was awarded a share of the Nobel Prize, along with Martin Ryle (1918–1984), for their work in radio astronomy. Fred Hoyle (1915–2001) and others have argued that Jocelyn Bell should have shared the prize as well; Hewish had designed the radio array and observational technique, but Bell was the first to notice the pulsar signal. This controversial omission has inspired references to the award as the “no-Bell” prize.

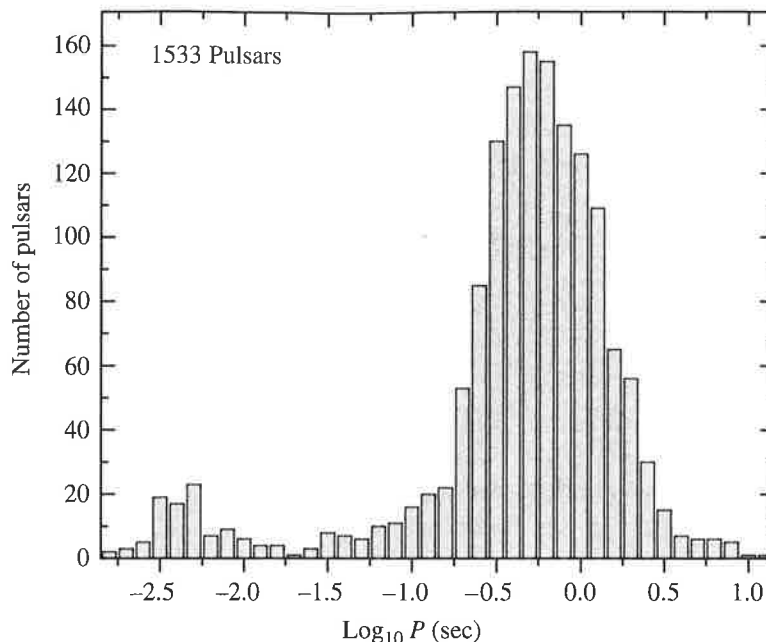


**FIGURE 16.14** The distribution of periods for 1533 pulsars. The millisecond pulsars are clearly evident on the left. The average period is about 0.795 s. (Data from Manchester, R. N., Hobbs, G. B., Teoh, A., and Hobbs, M., *A. J.*, 129, 1993, 2005. Data available at <http://www.atnf.csiro.au/research/pulsar/psrcat>.)

prefix (for Pulsating Source of Radio) followed by its right ascension ( $\alpha$ ) and declination ( $\delta$ ). For example, the source of Bell's scruff is PSR 1919+21, identifying its position as  $\alpha = 19^{\text{h}}19^{\text{m}}$  and  $\delta = +21^{\circ}$ .

### General Characteristics

All known pulsars share the following characteristics, which are crucial clues to their physical nature:

- Most pulsars have periods between 0.25 s and 2 s, with an average time between pulses of about 0.795 s (see Fig. 16.14). The pulsar with the longest known period is PSR 1841-0456 ( $P = 11.8$  s); Terzan 5ad (PSR J1748-2446ad) is the fastest known pulsar ( $P = 0.00139$  s).
- Pulsars have extremely well-defined pulse periods and would make exceptionally accurate clocks. For example, the period of PSR 1937+214 has been determined to be  $P = 0.00155780644887275$  s, a measurement that challenges the accuracy of the best atomic clocks. (Such precise determinations are possible because of the enormous number of pulsar measurements that can be made, given their very short periods.)
- The periods of all pulsars increase very gradually as the pulses slow down, the rate of increase being given by the period derivative  $\dot{P} \equiv dP/dt$ .<sup>31</sup> Typically,  $\dot{P} \approx 10^{-15}$ ,

<sup>31</sup>Note that  $\dot{P}$  is measured in terms of seconds of period change per second and so is unitless.

and the *characteristic lifetime* (the time it would take the pulses to cease if  $\dot{P}$  were constant) is  $P/\dot{P} \approx$  a few  $10^7$  years. The value of  $\dot{P}$  for PSR 1937+214 is unusually small,  $\dot{P} = 1.051054 \times 10^{-19}$ . This corresponds to a characteristic lifetime of  $P/\dot{P} = 1.48 \times 10^{16}$  s, or about 470 million years.

### Possible Pulsar Models

These characteristics enabled astronomers to deduce the basic components of pulsars. In the paper announcing their discovery, Hewish, Bell, and their co-authors suggested that an oscillating neutron star might be involved, but American astronomer Thomas Gold (1920–2004) quickly and convincingly argued instead that pulsars are rapidly rotating neutron stars.

There are three obvious ways of obtaining rapid regular pulses in astronomy:

1. **Binary stars.** If the orbital periods of a binary star system are to fall in the range of the observed pulsar periods, then extremely compact stars must be involved—either white dwarfs or neutron stars. The general form of Kepler's third law, Eq. (2.37), shows that if two  $1 M_{\odot}$  stars were to orbit each other every 0.79 s (the average pulsar period), then their separation would be only  $1.6 \times 10^6$  m. This is much less than the  $5.5 \times 10^6$  m radius of Sirius B, and the separation would be even smaller for more rapid pulsars. This eliminates even the smallest, most massive white dwarfs from consideration.

Neutron stars are so small that two of them could orbit each other with a period in agreement with those observed for pulsars. However, this possibility is ruled out by Einstein's general theory of relativity. As the two neutron stars rapidly move through space and time, gravitational waves are generated that carry energy away from the binary system. As the neutron stars slowly spiral closer together, their orbital period *decreases*, according to Kepler's third law. This contradicts the observed *increase* in the periods of the pulsars and so eliminates binary neutron stars as a source of the radio pulses.<sup>32</sup>

2. **Pulsating stars.** As we noted in Section 16.2, white dwarfs oscillate with periods between 100 and 1000 s. The periods of these nonradial g-modes are much longer than the observed pulsar periods. Of course, it might be imagined that a radial oscillation is involved with the pulsars. However, the period for the radial fundamental mode is a few seconds, too long to explain the faster pulses.

A similar argument eliminates neutron star oscillations. Neutron stars are about  $10^8$  times more dense than white dwarfs. According to the period–mean density relation for stellar pulsation (recall Section 14.2), the period of oscillation is proportional to  $1/\sqrt{\rho}$ . This implies that neutron stars should vibrate approximately  $10^4$  times more rapidly than white dwarfs, with a radial fundamental mode period around  $10^{-4}$  s and nonradial g-modes between  $10^{-2}$  s and  $10^{-1}$  s. These periods are much too short for the slower pulsars.

<sup>32</sup>Gravitational waves will be described in more detail in Section 18.6, as will the binary system of two neutron stars in which these waves have been indirectly detected.

3. **Rotating stars.** The enormous angular momentum of a rapidly rotating compact star would guarantee its precise clock-like behavior. But how fast can a star spin? Its angular velocity,  $\omega$ , is limited by the ability of gravity to supply the centripetal force that keeps the star from flying apart. This constraint is most severe at the star's equator, where the stellar material moves most rapidly. Ignore the inevitable equatorial bulging caused by rotation and assume that the star remains circular with radius  $R$  and mass  $M$ . Then the maximum angular velocity may be found by equating the centripetal and gravitational accelerations at the equator,

$$\omega_{\max}^2 R = G \frac{M}{R^2},$$

so that the minimum rotation period is  $P_{\min} = 2\pi/\omega_{\max}$ , or

$$P_{\min} = 2\pi \sqrt{\frac{R^3}{GM}}. \quad (16.29)$$

For Sirius B,  $P_{\min} \approx 7$  s, which is much too long. However, for a  $1.4 M_{\odot}$  neutron star,  $P_{\min} \approx 5 \times 10^{-4}$  s. Because this is a *minimum* rotation time, it can accommodate the complete range of periods observed for pulsars.

### Pulsars as Rapidly Rotating Neutron Stars

Only one alternative has emerged unscathed from this process of elimination, namely, that pulsars are rapidly rotating neutron stars. This conclusion was strengthened by the discovery in 1968 of pulsars associated with the Vela and Crab supernovae remnants. (Today dozens of pulsars are known to be associated with supernova remnants.) In addition, the Crab pulsar PSR 0531-21 has a very short pulse period of only 0.0333 s. No white dwarf could rotate 30 times per second without disintegrating, and the last doubts about the identity of pulsars were laid to rest. Until the discovery of the **millisecond pulsars** ( $P \approx 10$  ms or less) in 1982, the Crab pulsar held the title of the fastest known pulsar (see Fig. 16.14).<sup>33</sup> The Vela and Crab pulsars not only produce radio bursts but also pulse in other regions of the electromagnetic spectrum ranging from radio to gamma rays, including visible flashes as shown in Fig. 16.15. These young pulsars (and a few others) also display **glitches** when their periods abruptly *decrease* by a tiny amount ( $|\Delta P|/P \approx 10^{-6}$  to  $10^{-8}$ ); see Fig. 16.16.<sup>34</sup> These sudden spinups are separated by uneven intervals of several years.

### Geminga

The nearest pulsar yet detected is only some 90 pc away. PSR 0633+1746, nicknamed Geminga, was well known as a strong source of gamma rays for 17 years before its identity as a pulsar was established in 1992.<sup>35</sup> With a period of 0.237 s, Geminga pulses in both

<sup>33</sup>It is likely that the millisecond pulsars have rapid rotation periods that are a consequence of their membership in close binary systems; more than half of the known millisecond pulsars belong to binaries. For this reason, millisecond pulsars will be discussed in more detail in Section 18.6.

<sup>34</sup>See page 602 for a discussion of possible glitch mechanisms.

<sup>35</sup>*Geminga* means “does not exist” in Milanese dialect, accurately reflecting its long-mysterious nature.

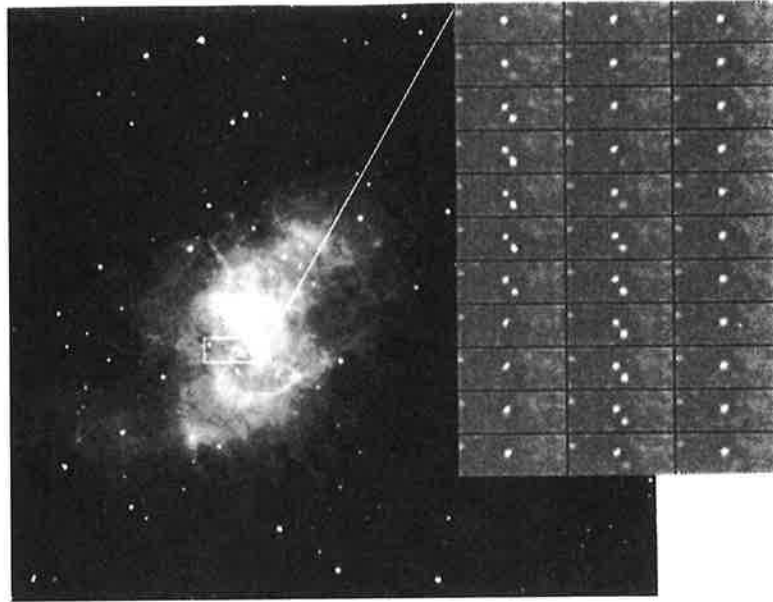


**FIGURE 16.15** A sequence of images showing the flashes at visible wavelengths from the Crab pulsar, located at the center of the Crab Nebula (left). A foreground star can be seen as the constant point of light above and to the left of the Crab pulsar. (Courtesy of National Optical Astronomy Observatories.)

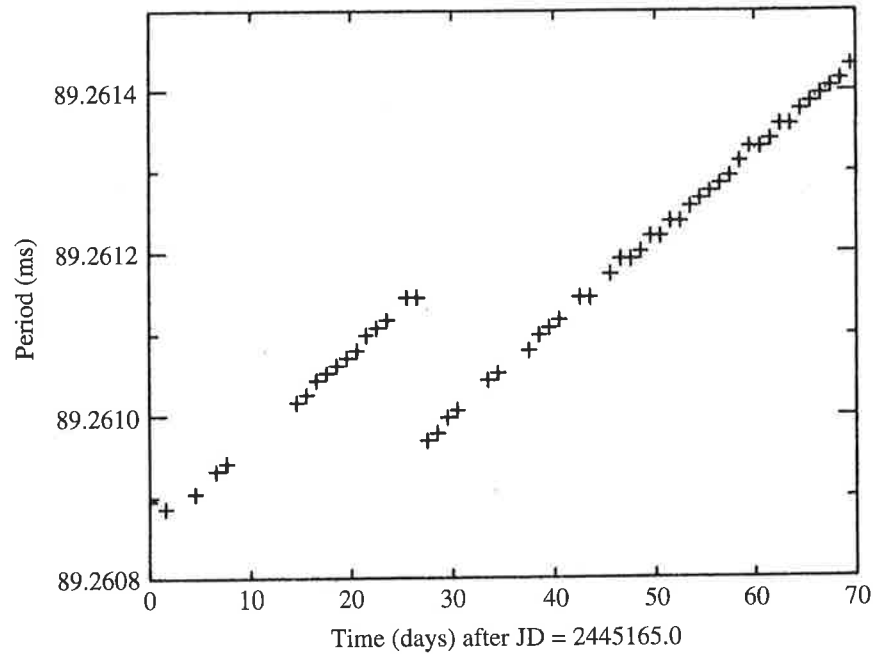


**FIGURE 16.16** A glitch in the Vela pulsar. (Figure adapted from McCulloch et al., *Aust. J. Phys.*, 40, 725, 1987.)

gamma and X-rays (but not at radio wavelengths) and may display glitches. In visible light, its absolute magnitude is fainter than +23.

### Evidence for a Core-Collapse Supernova Origin

Although at least one-half of all stars in the sky are known to be members of multiple-star systems, only a few percent of pulsars are known to belong to binary systems. Pulsars also move much faster through space than do normal stars, sometimes with speeds in excess of  $1000 \text{ km s}^{-1}$ . Both of these observations are consistent with a supernova origin for pulsars. This is because it is highly likely that a core-collapse supernova explosion is not perfectly spherically symmetric, so the forming pulsar could receive a kick, possibly ejecting it from any binary system that it may have been a part of initially. One hypothesis is that the pulsar is formed with an associated asymmetric jet and that, like a jet engine, the pulsar jet could launch the pulsar at high speed away from its formation point.

### Synchrotron and Curvature Radiation

Observations of the Crab Nebula, the remnant of the A.D. 1054 supernova, clearly reveal its intimate connection with the pulsar at its center. As shown in Fig. 16.15, the expanding nebula produces a ghostly glow surrounding gaseous filaments that wind throughout it. Interestingly, if the present rate of expansion is extrapolated backward in time, the nebula converges to a point about 90 years *after* the supernova explosion was observed. Obviously the nebula must have been expanding more slowly in the past than it is now, which implies that the expansion is actually accelerating.

In 1953, the Russian astronomer I. Shklovsky (1916–1985) proposed that the white light is **synchrotron radiation** produced when relativistic electrons spiral along magnetic field lines. From the equation for the magnetic force on a moving charge  $q$ ,

$$\mathbf{F}_m = q(\mathbf{v} \times \mathbf{B}),$$

the component of an electron's velocity  $\mathbf{v}$  perpendicular to the field lines produces a circular motion around the lines, while the component of the velocity along the lines is not affected; see Fig. 16.17. As they follow the curved field lines, the relativistic electrons accelerate and emit electromagnetic radiation. It is called synchrotron radiation if the circular motion around the field lines dominates or **curvature radiation** if the motion is primarily along the field lines. In both cases, the shape of the continuous spectrum produced depends on the energy distribution of the emitting electrons and so is easily distinguished from the spectrum of blackbody radiation.<sup>36</sup> The radiation is strongly linearly polarized in the plane of the circular motion for synchrotron radiation and is strongly linearly polarized in the plane of the curving magnetic field line for curvature radiation. As a test of his theory, Shklovsky predicted that the white light from the Crab Nebula would be found to be strongly linearly

<sup>36</sup>Both synchrotron and curvature radiation are sometimes called *nonthermal* to distinguish them from the thermal origin of blackbody radiation.

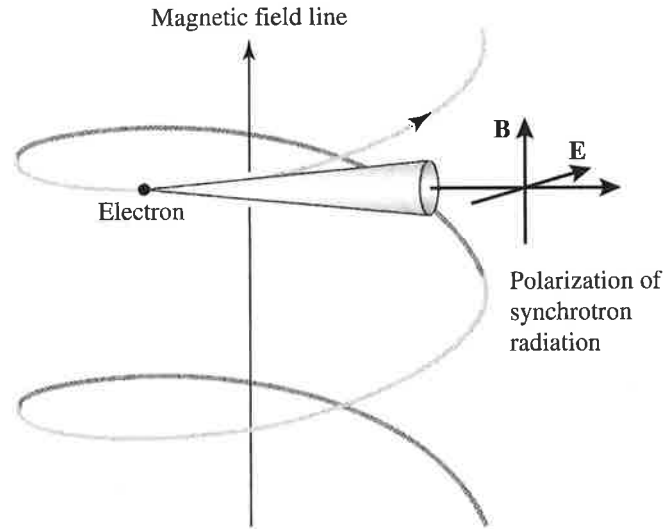


**FIGURE 16.17** Synchrotron radiation emitted by a relativistic electron as it spirals around a magnetic field line.

polarized. His prediction was subsequently confirmed as the light from some emitting regions of the nebula was measured to be 60% linearly polarized.

### The Energy Source for the Crab's Synchrotron Radiation

The identification of the white glow as synchrotron radiation raised new questions. It implied that magnetic fields of  $10^{-7}$  T must permeate the Crab Nebula. This was puzzling because, according to theoretical estimates, long ago the expansion of the nebula should have weakened the magnetic field far below this value. Furthermore, the electrons should have radiated away all of their energy after only 100 years. It is clear that the production of synchrotron radiation today requires both a replenishment of the magnetic field and a continuous injection of new energetic electrons. The total power needed for the accelerating expansion of the nebula, the relativistic electrons, and the magnetic field is calculated to be about  $5 \times 10^{31}$  W, or more than  $10^5 L_{\odot}$ .

The energy source is the rotating neutron star at the heart of the Crab Nebula. It acts as a huge flywheel and stores an immense amount of rotational kinetic energy. As the star slows down, its energy supply decreases.

To calculate the rate of energy loss, write the rotational kinetic energy in terms of the period and moment of inertia of the neutron star:

$$K = \frac{1}{2} I \omega^2 = \frac{2\pi^2 I}{P^2}.$$

Then the rate at which the rotating neutron star is losing energy is

$$\frac{dK}{dt} = -\frac{4\pi^2 I \dot{P}}{P^3}. \quad (16.30)$$

**Example 16.7.1.** Assuming that the neutron star is a uniform sphere with  $R = 10$  km and  $M = 1.4 M_{\odot}$ , its moment of inertia is approximately

$$I = \frac{2}{5}MR^2 = 1.1 \times 10^{38} \text{ kg m}^2.$$

Inserting  $P = 0.0333$  s and  $\dot{P} = 4.21 \times 10^{-13}$  for the Crab pulsar gives  $dK/dt \approx 5.0 \times 10^{31}$  W. Remarkably, this is exactly the energy required to power the Crab Nebula. The slowing down of the neutron star flywheel has enabled the nebula to continue shining and expanding for nearly 1000 years.

It is important to realize that this energy is not transported to the nebula by the pulse itself. The radio luminosity of the Crab's pulse is about  $10^{24}$  W, 200 million times smaller than the rate at which energy is delivered to the nebula. (For older pulsars, the radio pulse luminosity is typically  $10^{-5}$  of the spin-down rate of energy loss.) Thus the pulse process, whatever it may be, is a minor component of the total energy-loss mechanism.

Figure 16.18 shows an HST view of the immediate environment of the Crab pulsar. The ring-like halo seen on the west side of the pulsar is a glowing torus of gas; it may be the result of a polar jet from the pulsar forcing its way through the surrounding nebula. Just to the east of the pulsar, about 1500 AU away, is a bright knot of emission from shocked material in the jet, perhaps due to an instability in the jet itself. Another knot is seen at

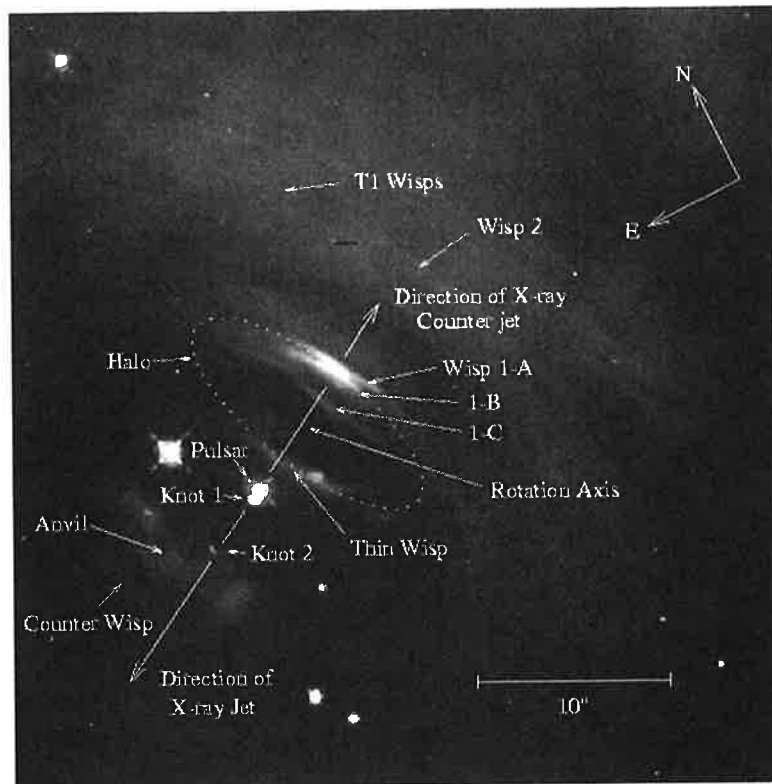


**FIGURE 16.18** An HST image of the immediate surroundings of the Crab pulsar. (Figure from Hester et al., *Ap. J.*, 448, 240, 1995.)

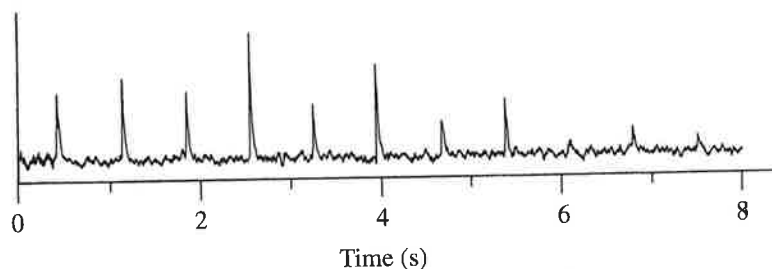
a distance of 9060 AU. Low time-resolution “movies” of the central region of the Crab supernova remnant obtained by long-term observations by HST and Chandra are actually able to show the expansion and evolution of that portion of the nebula. Some of the wisps appear to moving outward at between  $0.35c$  and  $0.5c$ .<sup>37</sup>

### The Structure of the Pulses

Before describing the details of a model pulsar, it is worth taking a closer look at the pulses themselves. As can be seen in Fig. 16.19, the pulses are brief and are received over a small fraction of the pulse period (typically from 1% to 5%). Generally, they are received at radio wave frequencies between roughly 20 MHz and 10 GHz.

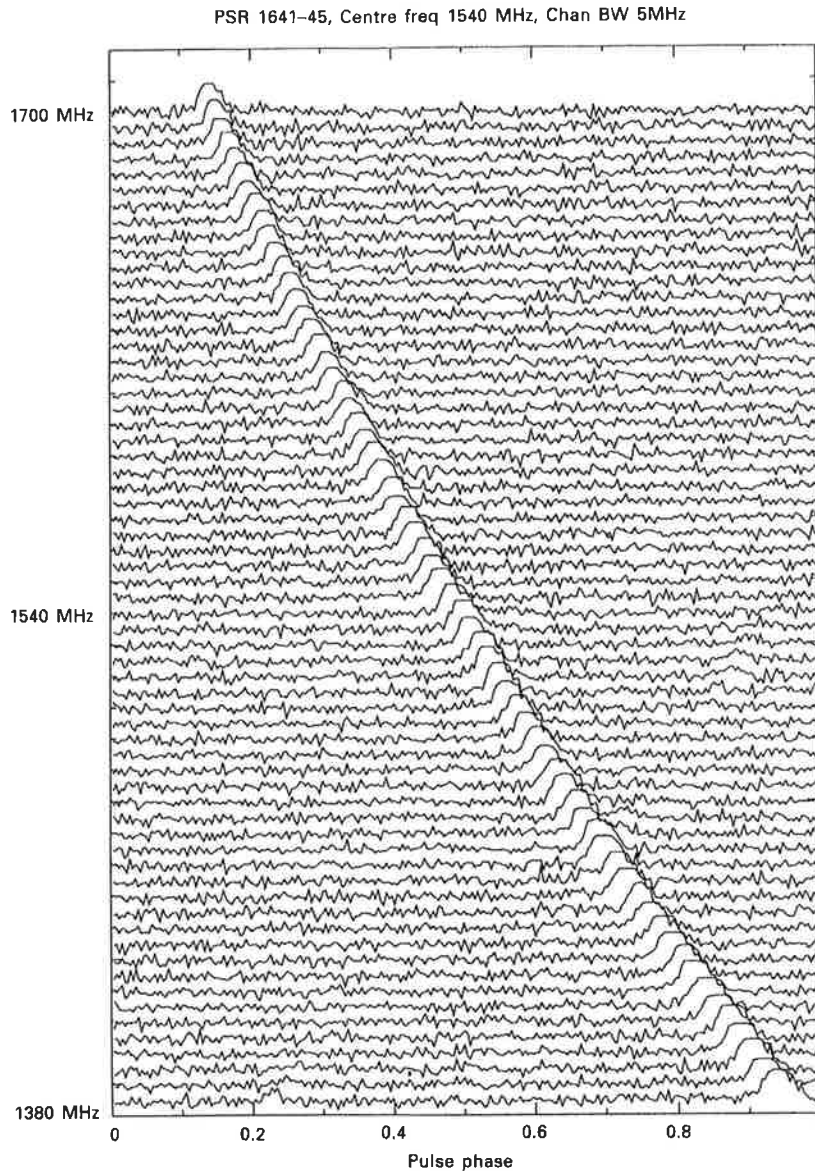
As the pulses travel through interstellar space, the time-varying electric field of the radio waves causes the electrons that are encountered along the way to vibrate. This process slows the radio waves below the speed of light in a vacuum,  $c$ , with a greater retardation at lower frequencies. Thus a sharp pulse emitted at the neutron star, with all frequencies peaking at the same time, is gradually drawn out or *dispersed* as it travels to Earth (see Fig. 16.20). Because more distant pulsars exhibit a greater pulse dispersion, these time delays can be used to measure the distances to pulsars. The results show that the known pulsars are concentrated within the plane of our Milky Way Galaxy (Fig. 16.21) at typical distances of hundreds to thousands of parsecs.

Figure 16.22 shows that there is a substantial variation in the shape of the individual pulses received from a given pulsar. Although a typical pulse consists of a number of brief *subpulses*, the *integrated pulse profile*, an average built up by adding together a train of 100 or more pulses, is remarkably stable. Some pulsars have more than one average pulse profile and abruptly switch back and forth between them (Fig. 16.23). The subpulses may appear at random times in the “window” of the main pulse, or they may march across in a phenomenon known as *drifting subpulses*, as shown in Fig. 16.24. For about 30% of all known pulsars, the individual pulses may simply disappear or *null*, only to reappear up to 100 periods later. Drifting subpulses may even emerge from a nulling event in step with those that entered the null. Finally, the radio waves of many pulsars are strongly linearly polarized (up to 100%), a feature that indicates the presence of a strong magnetic field.



**FIGURE 16.19** Pulses from PSR 0329+54 with a period of 0.714 s. (Figure adapted from Manchester and Taylor, *Pulsars*, W. H. Freeman and Co., New York, 1977.)

<sup>37</sup>See Hester, et al., *Ap. J.*, 577, L49, 2002. The movies are at <http://chandra.harvard.edu/photo/2002/0052/movies.html>.



**FIGURE 16.20** Dispersion of the pulse from PSR 1641-45. (Figure from Lyne and Graham-Smith, *Pulsar Astronomy*, ©Cambridge University Press, New York, 1990. Reprinted with the permission of Cambridge University Press.)

### The Basic Pulsar Model

The basic pulsar model, shown in Fig. 16.25, consists of a rapidly rotating neutron star with a strong dipole magnetic field (two poles, north and south) that is inclined to the rotation axis at an angle  $\theta$ . As explained in the previous section, the rapid rotation and the strong dipole field both arise naturally following the collapse of the core of a supergiant star.

First, we need to obtain a measure of the strength of the pulsar's magnetic field. As the pulsar rotates, the magnetic field at any point in space will change rapidly. According to Faraday's law, this will induce an electric field at that point. Far from the star (near the **light cylinder** defined in Fig. 16.26) the time-varying electric and magnetic fields form an electromagnetic wave that carries energy away from the star. For this particular situation,

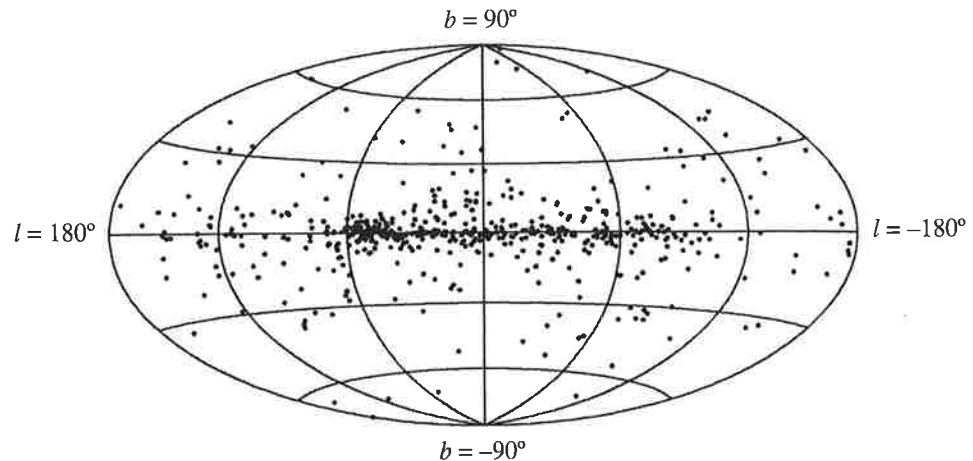


**FIGURE 16.21** Distribution of 558 pulsars in galactic coordinates, with the center of the Milky Way in the middle. The clump of pulsars at  $l = 60^\circ$  is a selection effect due to the fixed orientation of the Arecibo radio telescope. (Figure from Taylor, Manchester, and Lyne, *Ap. J. Suppl.*, 88, 529, 1993.)

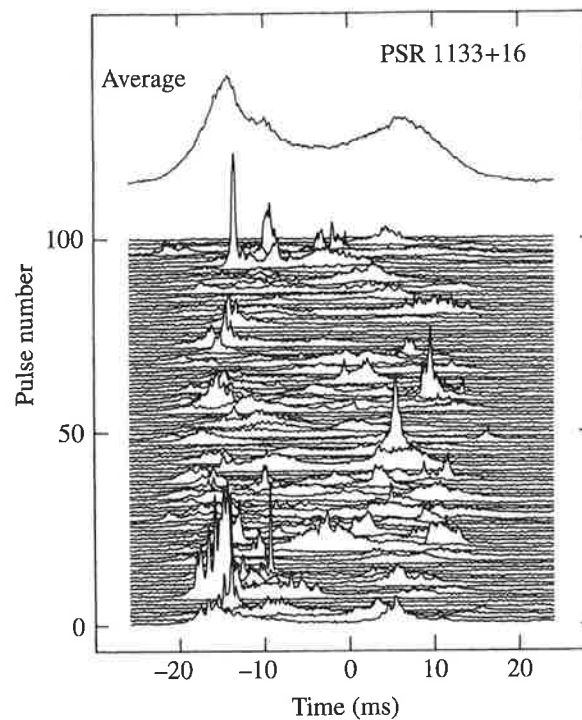


**FIGURE 16.22** The average of 500 pulses (top) and a series of 100 consecutive pulses (below) for PSR 1133+16. (Figure adapted from Cordes, *Space Sci. Review*, 24, 567, 1979.)

the radiation is called **magnetic dipole radiation**. Although it is beyond the scope of this book to consider the model in detail, we note that the energy per second emitted by the rotating magnetic dipole is

$$\frac{dE}{dt} = \frac{32\pi^5 B^2 R^6 \sin^2 \theta}{3\mu_0 c^3 P^4}, \quad (16.31)$$

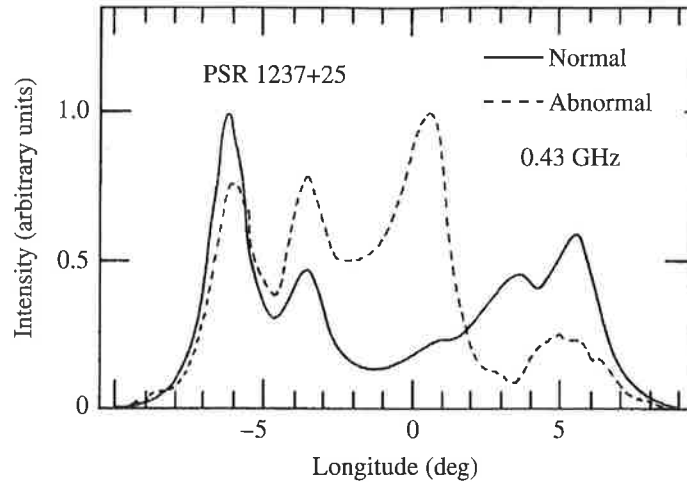


**FIGURE 16.23** Changes in the integrated pulse profile of PSR 1237+25 due to mode switching. This pulsar displays five distinct subpulses. (Figure adapted from Bartel et al., *Ap. J.*, 258, 776, 1982.)

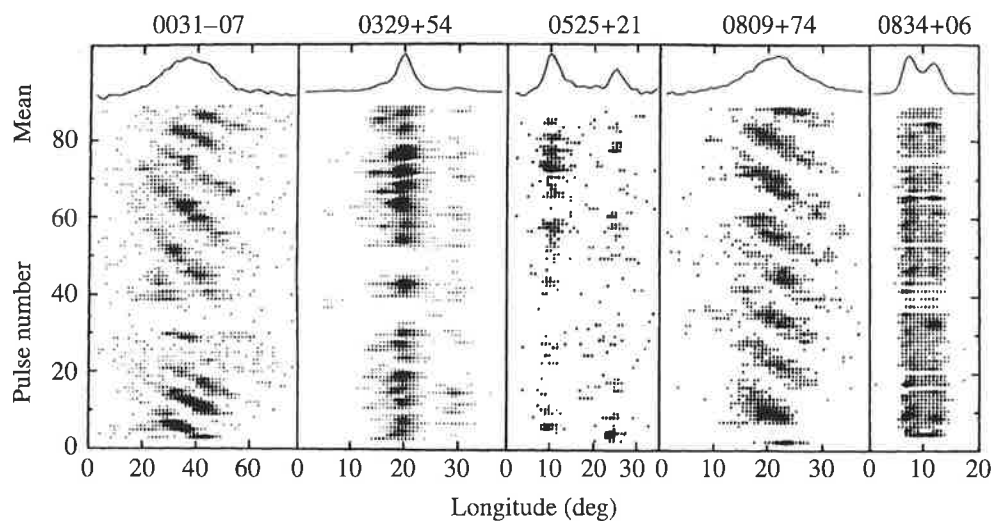


**FIGURE 16.24** Drifting subpulses for two pulsars; note that PSR 0031-07 also nulls. (Figure from Taylor et al., *Ap. J.*, 195, 513, 1975.)

where  $B$  is the field strength at the magnetic pole of the star of radius  $R$ . The minus sign indicates that the neutron star is drained of energy, causing its rotation period,  $P$ , to increase. Note that the factor of  $1/P^4$  means that the neutron star will lose energy much more quickly at smaller periods. Since the average pulsar period is 0.79 s, most pulsars are born spinning considerably faster than their current rates, with typical initial periods of a few milliseconds.

Assuming that all of the rotational kinetic energy lost by the star is carried away by magnetic dipole radiation,  $dE/dt = dK/dt$ . Using Eqs. (16.30) and (16.31), this is

$$-\frac{32\pi^5 B^2 R^6 \sin^2 \theta}{3\mu_0 c^3 P^4} = -\frac{4\pi^2 I \dot{P}}{P^3}. \quad (16.32)$$

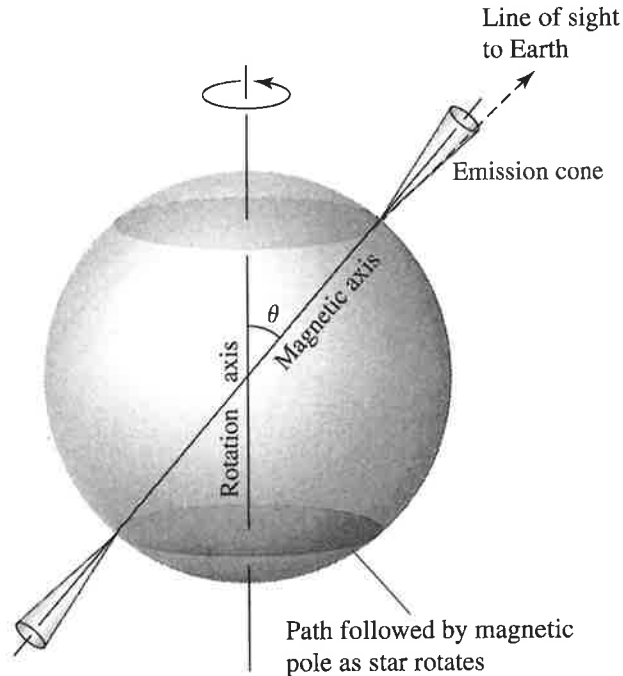


FIGURE 16.25 A basic pulsar model.

This can be easily solved for the magnetic field at the pole of the neutron star,

$$B = \frac{1}{2\pi R^3 \sin \theta} \sqrt{\frac{3\mu_0 c^3 I P \dot{P}}{2\pi}}. \quad (16.33)$$

**Example 16.7.2.** We will estimate the magnetic field strength at the poles of the Crab pulsar (PSR 0531-21), with  $P = 0.0333$  s and  $\dot{P} = 4.21 \times 10^{-13}$ . Assuming that  $\theta = 90^\circ$ , Eq. (16.33) then gives a value of  $8.0 \times 10^8$  T. As we have seen, the Crab pulsar is interacting with the dust and gas in the surrounding nebula, so there are other torques that contribute to slowing down the pulsar's spin. This value of  $B$  is therefore an overestimate; the accepted value of the Crab pulsar's magnetic field is  $4 \times 10^8$  T.<sup>38</sup> Values of  $B$  around  $10^8$  T are typical for most pulsars.

However, repeating the calculation for PSR 1937+214 with  $P = 0.00156$  s,  $\dot{P} = 1.05 \times 10^{-19}$ , and assuming the same value for the moment of inertia, we find the magnetic field strength to be only  $B = 8.6 \times 10^4$  T. This much smaller value distinguishes the millisecond pulsars and provides another hint that these fastest pulsars may have a different origin or environment.

### Correlation Between Period Derivatives and Pulsar Classes

Figure 16.27 shows the distribution of period derivatives for pulsars as a function of pulsar period. Although the vast majority of pulsars fall into a large grouping in the middle of

<sup>38</sup>The suggestion that the Crab Nebula is powered by the magnetic dipole radiation from a rotating neutron star was made by the Italian astronomer Franco Pacini in 1967, a year *before* the discovery of pulsars!

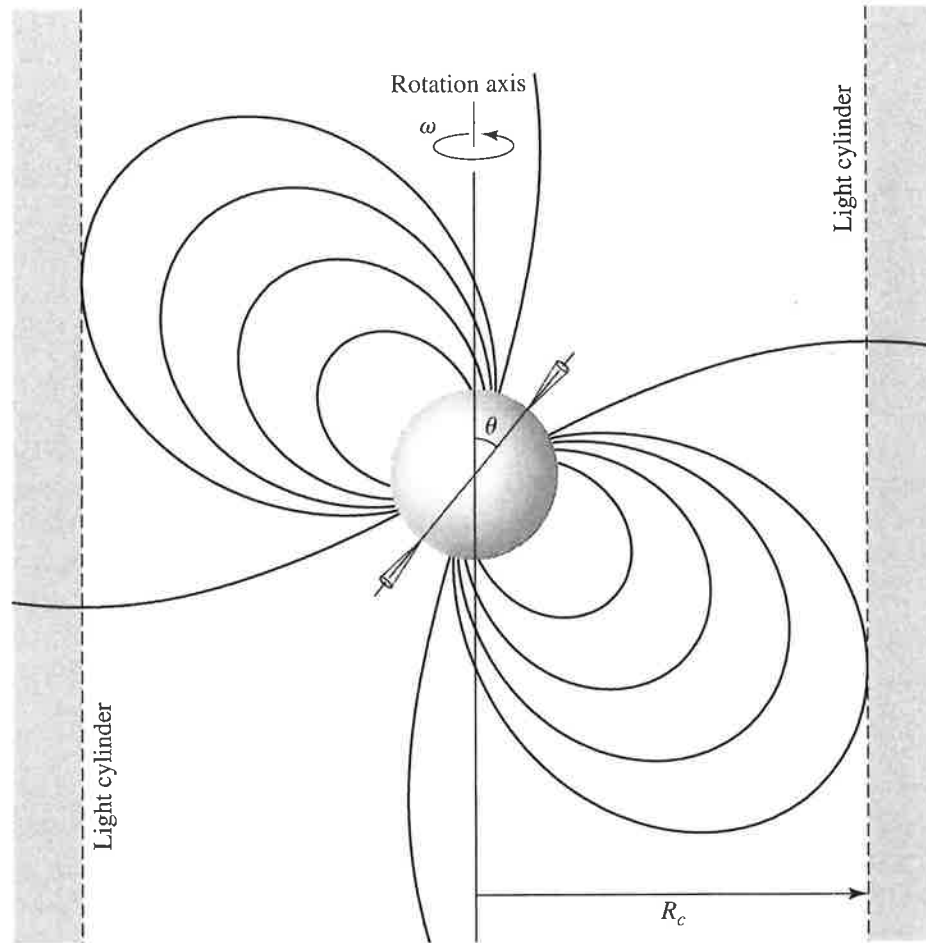


**FIGURE 16.26** The light cylinder around a rotating neutron star. The cylinder's radius  $R_c$  is where a point co-rotating with the neutron star would move at the speed of light:  $R_c = c/\omega = cP/2\pi$ .

the plot, the millisecond pulsars show a clear correlation with pulsars known to exist in binary systems. Other classes of pulsars are also evident: Pulsars known to emit energy at X-ray wavelengths have the longest periods and have the largest period derivatives, whereas high-energy pulsars that emit energies from radio frequencies through the infrared or higher frequencies tend to have larger values of  $\dot{P}$  but otherwise typical periods. Note that although nearly all of the pulsars represented in Fig. 16.27 have positive values of  $\dot{P}$ , some of them, primarily the binary pulsars, actually have values of  $\dot{P} < 0$ , meaning that their periods are decreasing (they are speeding up!). Figure 16.27 may be compared with the histogram of pulsar periods shown in Fig. 16.14.

### Toward a Model of Pulsar Emission

Developing a detailed model of the pulsar's emission mechanism has been an exercise in frustration because almost every observation is open to more than one interpretation. The emission of radiation is the most poorly understood aspect of pulsars, and at present there is agreement only on the most general features of how a neutron star manages to produce radio waves. The following discussion summarizes a popular model of the pulse process.

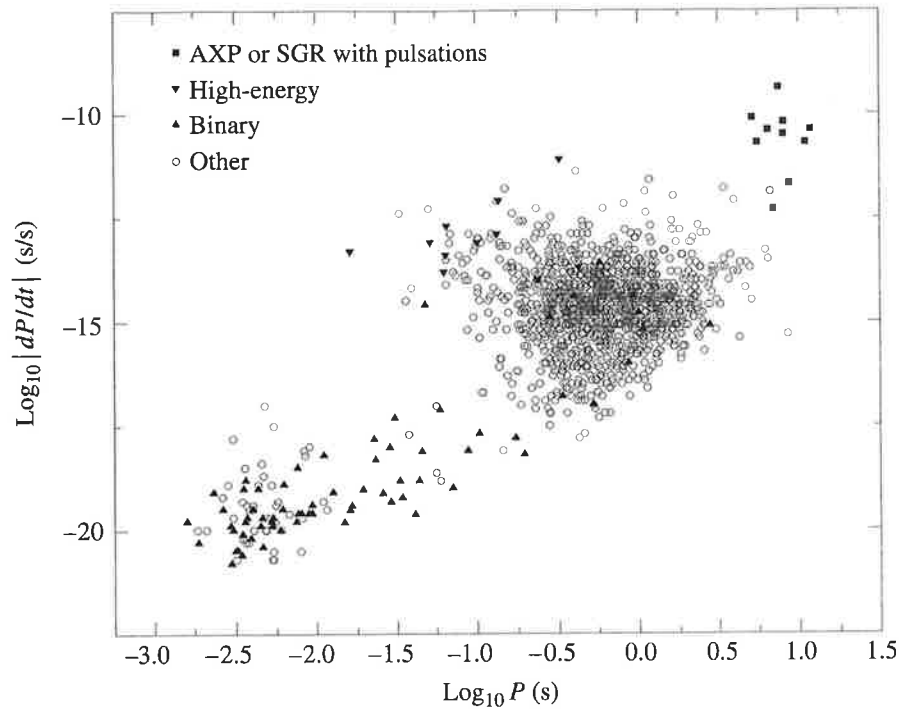


**FIGURE 16.27** The absolute value of the time derivative of period ( $|\dot{P}|$ ) versus period ( $P$ ) for all pulsars for which  $\dot{P}$  has been determined. Special classes of pulsars are depicted separately: Anomalous X-ray pulsars (AXP) or Soft Gamma Repeaters (SGR) with pulsations, high-energy pulsars with emitted frequencies between radio and infrared or higher, and binary pulsars (with one or more known binary companions) are depicted separately. All remaining pulsars are indicated as “other.” Note the abundance of known binary pulsars among the millisecond pulsars. (Data from Manchester, Hobbs, Teoh, and Hobbs, *A. J.*, 129, 1993, 2005. Data available at <http://www.atnf.csiro.au/research/pulsar/psrcat>.)

You should keep in mind, however, that there is as yet no general consensus on whether the object being discussed actually occurs in nature or only in the minds of astrophysicists!

It is at least certain that the rapidly changing magnetic field near the rotating pulsar induces a huge electric field at the surface. The electric field of about  $6.3 \times 10^{10} \text{ V m}^{-1}$  easily overcomes the pull of gravity on charged particles in the neutron star’s crust. For example, the electric force on a proton is about 300 million times stronger than the force of gravity, and the ratio of the electric force on an electron to the gravitational force is even more overwhelming. Depending on the direction of the electric field, either negatively charged electrons or positively charged ions will be continuously ripped from the neutron star’s polar regions. This creates a **magnetosphere** of charged particles surrounding the pulsar that is dragged around with the pulsar’s rotation. However, the speed of the co-rotating particles cannot exceed the speed of light, so at the light cylinder the charged particles are spun away, carrying the magnetic field with them in a pulsar “wind.” Such a wind may be responsible for the replenishment of the Crab Nebula’s magnetic field and the continual delivery of relativistic particles needed to keep the nebula shining.

The charged particles ejected from the vicinity of the pulsar’s magnetic poles are quickly accelerated to relativistic speeds by the induced electric field. As the electrons follow the

curved magnetic field lines, they emit curvature radiation in the form of energetic gamma-ray photons. This radiation is emitted in a narrow beam in the instantaneous direction of motion of the electron, a consequence of the relativistic headlight effect discussed in Section 4.3. Each gamma-ray photon has so much energy that it can spontaneously convert this energy into an electron–positron pair via Einstein’s relation  $E = mc^2$ . (This process, described by  $\gamma \rightarrow e^- + e^+$ , is just the inverse of the annihilation process mentioned in Section 10.3 for the Sun’s interior.) The electrons and positrons are accelerated and in turn emit their own gamma rays, which create more electron–positron pairs, and so on. A cascade of pair production is thus initiated near the magnetic poles of the neutron star. Coherent beams of curvature radiation emitted by bunches of these particles may be responsible for the individual subpulses that contribute to the integrated pulse profile.

As these particles continue to curve along the magnetic field lines, they emit a continuous spectrum of curvature radiation in the forward direction, producing a narrow cone of radio waves radiating from the magnetic polar regions.<sup>39</sup> As the neutron star rotates, these radio waves sweep through space in a way reminiscent of the light from a rotating lighthouse beacon. If the beam happens to fall on a radio telescope on a blue-green planet in a distant Solar System, the astronomers there will detect a regular series of brief radio pulses.

As the pulsar ages and slows down, the structure of the underlying neutron star must adapt to the reduced rotational stresses. As a consequence, perhaps the crust settles a fraction of a millimeter and the star spins faster as a result of its decreased moment of inertia, or perhaps the superfluid vortices in the neutron star’s core become momentarily “unpinned” from the underside of the solid crust where they are normally attached, giving the crust a sudden jolt. Either possibility could produce a small but abrupt increase in the rotation speed, and the astronomers on Earth would record a glitch for the pulsar (recall Fig. 16.16).

The question of a pulsar’s final fate, as its period increases beyond several seconds, has several possible answers. It may be that the neutron star’s magnetic field, originally produced by the collapse of the pre-supernova star’s degenerate stellar core, decays with a characteristic time of 9 million years or so. Then, at some future time when the pulsar’s period has been reduced to several seconds, its magnetic field may no longer be strong enough to sustain the pulse mechanism, and the pulsar turns off. On the other hand, it may be that the magnetic field does not decay appreciably but is maintained by a dynamo-like mechanism involving the differential rotation of the crust and core of the neutron star. However, rotation itself is an essential ingredient of any pulsar emission mechanism. As a pulsar ages and slows down, its beam will become weaker even if the magnetic field does not decay. In this case, the radio pulses may become too faint to be detected as the pulsar simply fades below the sensitivity of radio telescopes. The timescale for the decay of a neutron star’s magnetic field is a matter of considerable debate, and both scenarios are consistent with the observations.

### Magnetars and Soft Gamma Repeaters

The preceding sketch reflects the current state of uncertainty about the true nature of pulsars. There are few objects in astronomy that offer such a wealth of intriguing observational detail

<sup>39</sup>The visible, X-ray, and gamma-ray pulses received from the Crab, Vela, Circinus, and Geminga pulsars may originate farther out in the pulsar’s magnetosphere.

and yet are so lacking in a consistent theoretical description. Regardless of whether the basic picture outlined is vindicated or is supplanted by another view (perhaps involving a disk of material surrounding the neutron star), pulsar theorists will continue to take advantage of this unique natural laboratory for studying matter under the most extreme conditions.

To complicate the picture further, it is now believed that a class of extremely magnetic neutron stars known as **magnetars** exists. Magnetars have magnetic field strengths that are on the order of  $10^{11}$  T, several orders of magnitude greater than typical pulsars. They also have relatively slow rotation periods of 5 to 8 seconds. Magnetars were first proposed to explain the **soft gamma repeaters** (SGRs), objects that emit bursts of hard X-rays and soft gamma-rays with energies of up to 100 keV (recall Fig. 16.27). Only a few SGRs are known to exist in the Milky Way Galaxy, and one has been detected in the Large Magellanic Cloud. Each of the SGRs is also known to correlate with supernova remnants of fairly young age ( $\sim 10^4$  y). This would suggest that magnetars, if they are the source of the SGRs, are short-lived phenomena. Perhaps the Galaxy has many "extinct," or low-energy, magnetars scattered through it.

The emission mechanism of intense X-rays from SGRs is thought to be associated with stresses in the magnetic fields of magnetars that cause the surface of the neutron star to crack. The resulting readjustment of the surface produces a *super-Eddington* release of energy (roughly  $10^3$  to  $10^4$  times the Eddington luminosity limit in X-rays). In order to obtain such high luminosities, it is believed that the radiation must be confined; hence the need for very high magnetic field strengths.

Magnetars are distinguished from ordinary pulsars by the fact that the energy of the magnetar's field plays the major role in the energetics of the system, rather than rotation, as is the case for pulsars. Clearly much remains to be learned about the exotic environment of rapidly rotating, degenerate spheres with radii on the order of 10 km and densities exceeding the density of the nucleus of an atom.

## SUGGESTED READING

### General

Burnell, Jocelyn Bell, "The Discovery of Pulsars," *Serendipitous Discoveries in Radio Astronomy*, National Radio Astronomy Observatory, Green Bank, WV, 1983.

Graham-Smith, F., "Pulsars Today," *Sky and Telescope*, September 1990.

Kawaler, Stephen D., and Winget, Donald E., "White Dwarfs: Fossil Stars," *Sky and Telescope*, August 1987.

Nather, R. Edward, and Winget, Donald E., "Taking the Pulse of White Dwarfs," *Sky and Telescope*, April 1992.

Trimble, Virginia, "White Dwarfs: The Once and Future Suns," *Sky and Telescope*, October 1986.

### Technical

Clayton, Donald D., *Principles of Stellar Evolution and Nucleosynthesis*, University of Chicago Press, Chicago, 1983.